



UNIVERSITY OF TRENTO

DIPARTIMENTO DI INGEGNERIA INDUSTRIALE
Corso di Laurea Magistrale in Ingegneria Meccatronica

Autonomous VTOL for avalanche buried searching Avionics

Candidato:
Matteo Ragni
Matricola 161822

Relatori:
Prof. Ing. Paolo Bosetti
Prof. Ing. Francesco Biral

Anno Accademico 2013–2014

To my family and Laura

Abstract

The aim of the thesis is to inspect and derive a model for an autonomous VTOL that could help Mountain Rescue in finding the position of buried person under avalanche.

The first part of the thesis will inspect the state of the art in buried searching, ARTVA transmitter and searching algorithms. Also we will show some of the requirements and technical specifications for a searching drone.

In the second chapter we will expose the problem of searching the position of a transmitting source in near-field with ferromagnetic antennas. The chapter will be closed with a design for a digital ARTVA receiver

In the third chapter, a new kind of searching algorithm will be defined, including routines of obstacle-avoidance and altitude-keeping.

In the fourth chapter, a model of an hexa-copter and its stabilization controls are derived and simulated in MATLAB/Simulink. The loop is closed on some of the searching algorithm defined in the previous chapter. Results of searching routine are shown and critically examined.

The last chapter will take into account all the results to derive some conclusions about the stated problem, with some suggestions for further improvements.

There are so many person that helped me through this journey, that I should write an entire thesis only to name them all. But few of them actively suggested me the solution that you find in this text. First of all, Ermes Floriani, that started this project; the men and women of Italian Mountain Rescue Team, that risk their life every day to save person in danger, and helped us in finding information for develop a drone that could be really helpful; Ing. Paolo Bosetti and Ing. Francesco Biral that always believed and inspired me during the Master Course; Luigi Ghinassi, who gave me the intellectual instruments to understand and develop an ARTVA prototype; Matteo Cocetti, that has shared with me his genuine and innate mastering of mathematics and problem solving; my father that has always tried to find a solution for some of the usolveable problem that I've encountered.

There are many others, maybe not cited here, but firmly present in my heart. Thank you all. The complete

sources of this thesis are available at: <https://github.com/MatteoRagni/MasterThesis>

The complete sources of the MATLAB/Simulink project are available at: <https://github.com/AvalancheMustache/ArtvaSearchAlgorithm>

Contents

1 Introduction to Mountain Rescue	11
1.1 Some statistics about the avalanche accidents	12
1.2 Avalanche Beacons	12
1.3 State of the Art	14
1.4 Autonomous VTOL for buried searching	17
2 Design of a digital ARTVA	21
2.1 Analysis of transmitting pattern	22
2.2 Analytical signal analysis - A1–A	28
2.3 Receiving antenna	29
2.4 Digital ARTVA prototype	32
2.5 Appendix	38
3 Drone Avionics	43
3.1 Perception Action paradigm	44
3.2 Building the PA map of the drone	46
3.3 Hexa-copter model	47
3.4 Obstacle avoidance	53
3.5 Altitude keeping	56
3.6 The signal detection problem	59
3.7 Searching for the signal	63
3.8 Source searching algorithm	65
4 Simulations	69
4.1 Implementations	69
4.2 Results	72
List of symbols	79
Bibliography	81

1

Introduction to Mountain Rescue

Contents

1.1	Some statistics about the avalanche accidents	12
1.2	Avalanche Beacons	12
1.2.1	Transmission Mode	13
1.2.2	Receiving Mode	13
<i>Analog Beacons</i>	13
<i>Digital Beacons</i>	13
1.2.3	Italian Mountain Rescue Intervention	13
<i>Intervention on Avalanche</i>	13
<i>Equipment</i>	14
1.3	State of the Art	14
1.3.1	Transmission	14
1.3.2	Reception	15
1.3.3	Searching Algorithms	16
<i>The magnetic momentum problem</i>	16
<i>Multiple Burial</i>	16
<i>A complex procedure</i>	17
1.4	Autonomous VTOL for buried searching	17
1.4.1	Why the use of a VTOL?	17
1.4.2	Quality Function Deployment	18
<i>Customer Needs</i>	18
<i>Technical Specification</i>	18
<i>Merging the tables and comparison</i>	19
<i>Components selection</i>	19

Many people in the last few year have re-discovered a passion for winter mountain sports. Some of them have decided to explore the extreme version of this sports, like winter climbing or free-riding.

The increasing number of riders in extreme snow condition facilitates avalanches falling. Mountain Rescue Team is often called for search probable buried hikers, constrained to operate in an environment with an high residual risk. To facilitate the research, national and regional laws¹ have imposed the use of ARTVA transmitter, also called *Avalanche Beacons*, for rider of non-equipped trails.

¹ Repubblica Italiana. Legge 24/12/2003 n. 363. Gazzetta Ufficiale, 2003

1.1 Some statistics about the avalanche accidents

A.I.NE.VA: from the Italian *Associazione Interregionale NEve e VAlanghe*

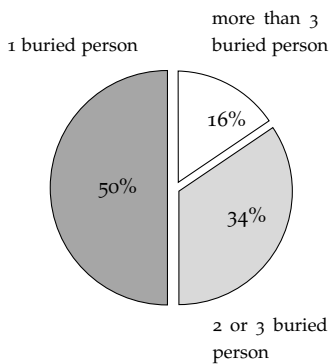


Figure 1.1: Number of buried

During the year 2000, alpine countries decided to start an on line Database of avalanche victims, with the participation of the Italian council called A.I.NE.VA.. The statistics show a mean of 18 victims per year in Italy. The number of accident is clearly related to the higher number of avalanche phenomena, strongly associated to the rising number of riders that are using snowboard.

A deeper analysis of the data shows that the 40% of the accidents have victims. Also, the number of buried was analyzed. Statistically:

- 50% of the accidents have only one buried
 - 34% of the accidents have two or three buried
 - 16% of the accidents have four or more or more buried
- Another important factor is the position of the overwhelms hikers:
- 37% remain on the surface of the avalanche
 - 28% are only partially buried
 - 35% are completely buried

The survival curve, because of frostbite and hypothermia, without considerable traumas, has an upper limit of 15–18 minutes. Here is the the companion rescue that makes the real difference².

² Aa. Vv. *Club Alpino Italiano - Manuale Sci Alpinismo*. Commissione Pubblicazioni CAI, 2004

ARTVA: from the Italian *Apparecchio Ricerca Travolti VAlanga*

One last important statistic is the number of hikers found with the ARTVA. Considering the fact that the statistics do not take into account the episode of auto-rescue, the 7% of the buried are found by the use of the receivers, a very small amount of the total. This data should be revised in the light of the advent of new digital ARTVA receivers, that simplify the searching method, and reduce the searching time [11].

As reported in [6], within Europe and North America, avalanche airbags and avalanche transceiver reduce mortality, and companion rescue reduces incredibly the median duration of burial, remarking the extreme importance of those device for all mountaineers.

It is also known that 95% of complete burial are in the layer between –3 and 0 m of the avalanche.

1.2 Avalanche Beacons

There are two main typologies of avalanche transceiver. Differences are mostly in the user interface during receiving. We can divide in *analog* and *digital* ARTVA. Both device are equal for what concerns transmission. ARTVA can not be at the same time in transmission mode and receiving mode. Some models switch from receiving to transmission status after a scheduled amount of time.

1.2.1 Transmission Mode

During transmission, beacons transmit a so-called *wild-life tag*, or more simply, an intermittent signal at defined frequency, as stated in normative³. From the normative, it is possible to extract more informations about the transmitted signal, that are listed in section 2.2.

³ ETSI EN 300 718-(1 2 3 4). E.r.m. avalanche beacons - transmitter-receiver systems. Technical report, ETSI, 2001

1.2.2 Receiving Mode

The normative states for receiver:

- the $(S + N)/N$ ratio of 6dB at the terminal of electro-acoustic transducer
- a clear optical indication of direction for beacon with optical signal indication of direction

Analog Beacons

The analog beacon uses a cascade of filters and an identification circuit to extract the strength information of received signal. The strength is thus used as gain command for a sound generator, that rescuer uses to identify the direction of arrival. Typically, those ARTVA have a volume knob to perform a fine search. The main drawback is the extreme difficulty to perform a fast search, that requires an experienced user. Quoting [10]: *a better term for analog beacon would be audible-based*

Digital Beacons

Those beacons implements an user interface that indicates *the field line direction and an artificial distance to the center of the field*. This simplicity makes those beacons perfect for unexperienced user and auto-rescue: those device are **strongly advised by the Mountain Rescue for all hikers, experienced or not**.

Must be noted that the algorithm inside those transceivers runs on a very low power DPS, due to energy harvesting requirements, so often the rescuer must slow down his speed to gave time to the beacon to analyze received data. Also, it was pointed out from manufacturers that advanced techniques, like multi-buried identification and buried status (hearth-beat) make use of frequencies different from the one described in normative.

The Italian authority in Mountain Rescue is *Soccorso Alpino e Speleologico Italiano*



Figure 1.2: Tracker DTS Avalanche Transceiver, a digital beacon

1.2.3 Italian Mountain Rescue Intervention

What happens after an avalanche? We interviewed some of the professionals of the Mountain Rescue Team in province of Trento, and asked them to explain us the actual procedure.

Intervention on Avalanche

The intervention begin after a witness call. Usually the witness is one of the hikers that is on the accident location. In the best situation, the witness begins the companion rescue procedure, with his own avalanche beacon, and calls the emergency number.

During the emergency call, the operator tries to understand the location, alerts the rescue team on shift and tries to figure out the general situation that the team may encounter. A rescue unit is formed by:

- Mountain Rescue heli-ambulance expert
- Mountain Rescue canine unit
- Health equip and nurse

If heli-ambulance is cleared to take off, those are the first rescuers on the avalanche. The clearance is related to weather and light conditions, because flight is performed by eye-sight. If heli-ambulance mission is aborted, Mountain Rescue team have to reach the avalanche with ground vehicle.

Under certain strict condition, it is possible to perform an ARTVA search from the helicopter.

Once arrived on the location, if residual risk make it possible, the rescue team is dropped from the heli-ambulance and starts the searching procedure, with canine unit and with personal ARTVAs. The rescuers with the beacons follow a scheme that allow them to cover the avalanche front. This scheme is called primary search. While a signal is identified, the rescuer start a fine search to pinpoint the buried position.

Equipment

There is a procedural and moral obligation in having the last generation device, even if does not exist a directive that defines a specific model for the equipment. Each rescuer has a VHF transmitter and cellphone, along with the personal beacon.

It is possible to perform a search with other technology, like RECCO⁴, even if the detector is heavy and not always reliable.

1.3 State of the Art

In this section we will analyze the state of the art in the field of beacons construction and signal analysis.

1.3.1 Transmission

Normative states the use of a very long wavelength (λ) (656m). Such a long wavelength reduces the interference effects of snow, body and rocks and also multi-bouncing and multi-path effects[3] that may afflict some shorter waves. This is one of the main reason why GPS technology never erupted in this field[10].

This advantage also bring a consistent number of drawbacks, such

⁴ RECCO is a passive searching method, composed by a reflector included in hikers clothing, and a detector used by rescue teams. A RECCO detector usually performs passive search and 457kHz avalanche beacons search at the same time. The last generation detector has an average weight of 1kg, while the reflector weights only few grams. RECCO cannot be used for companion rescue

as the fact that the search is always performed in near-field (distance less of $\lambda/2\pi$). In the near-field, as we will see, interpretation of flux lines is quite complex, and it is difficult to derive a general direction of arrival algorithm.

Avalanche transceiver for companion rescue has to be small, therefore antennas and batteries has to be small. As we will see in the next chapter, to increase receiver antenna gain (also called effective height h_{eff}), ferrite core antennas are commonly used, but the efficiency and the noise introduced is not good. Those brings to transmitter that may be identified in the range of 40 to 60m, in function of type of receiver.

There is no big evolution in transmitters; almost all devices implement a simple amplitude-shifting-key (ASK) transmitter, build with an oscillator for the carrier, and a variable gain amplifier that modulates the intelligence signal.

1.3.2 Reception

Usually, an analog receiver has a little more bigger receiving radius with respect to a digital one. This difference is due to stronger filtration routines implemented in digital ARTVA, with respect to analog, and because of the dimension of the z-axis antenna.

A digital ARTVA implements multiple antennas. Some typical configurations are:

- two crossing antennas
- three perpendicular antennas

The signal from whips are preprocessed using analog circuitry and then converted and processed in a DSP microprocessor. There are some advanced techniques[18] implemented for the identification of the direction of the vectorial H-field, and also to help hikers and rescuers to find a transmitter.

In general, the circuit may be resumed as follows:

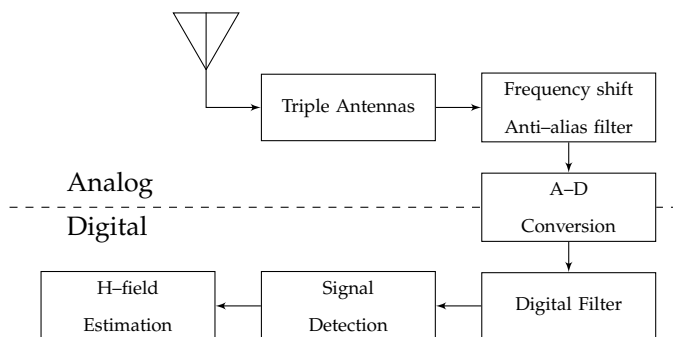


Figure 1.3: Block diagram of a commercial digital beacon, taken from [18]

- signal is received through the antennas
- the first stage of filtering is a frequency shift and an anti-aliasing filter, that is necessary to avoid problems during AD-conversion
- the signal is converted in the digital domain

- other filtration techniques are analyzed in [18], and are one of the main research topic in this field, in association with phase analysis to better understand the direction of the single components of the H-field
- the signal detector and magnetic field estimator is implemented via software

One of the main challenge is the problem of the noise introduced by antennas. This noise is proportional to the received signal, phenomenon that induces an unsurmountable issue in the identification of multiple burial signal.

1.3.3 Searching Algorithms

The magnetic momentum problem

The main problem is the searching of the burial. Until now, only few are the example of automatic searching, while quite consolidated is the practice of the manual searching. One of the key aspects is the problem of the orientation of the transmitter: as we will see in the next chapter, the direction of the transmitter antenna change radically the shape of the field. From a general point of view, with respect to classical far-field identification problem, in this case we have to identify 6 state for each transmitter⁵, instead of 3, while we can only collect 3 measurements (the H-field vector components).

Even if there are some solutions for near-field qualitative direction of arrival, as explained in detail in [12], typically those algorithms require a very prohibitive electro-mechanical circuitry, not suitable as mountain equipment (or in our case, a drone).

So far, only one solution earns the right to be cited: the solution proposed in [16, 17], based upon Bayesian estimation theory and Kalman filters, is a remarkable attempt to find new approach to this problem, even if based on the weak assumption of a perfect knowledge of the covariance matrix related to the noise. One step ahead in this direction should be the redefinition of the problem in a dual form, from the Kalman filter to the information filter, in which the complete uncertainty is presented with a null matrix of the canonical form, instead of a infinite-valued matrix of the normal form.

Multiple Burial

Those algorithms do not analyze the problem of multiple burial, and the subsequent possible situation of overlapping signal. An almost complete dissertation about this problem, with some test on beacon present on the market, may be found in [14, 7]. From those technical documents, distributed by one of the most well-know company in snow-safety, rises the evident lack of a solution for the overlapping problem, due to transmitted signal limitation. The most suggest solution is to run-away from an identified source in the hope to find another new signal. Some producer try to avoid this using parallel carrier frequency with additional information coded into intelligence

⁵ 3 states refer to the position of the transmitter, while the latter 3 refers to the magnetic dipole momentum that is parallel to the axis of the antenna

signal (unique ID, heartbeat status, ...). Those alternative frequencies are device/model dependent.

A complex procedure

Standard de facto is an algorithm of flux line following, in parallel with different assumption that user shall analyze, to derive the possible orientation of the buried person transmitting antenna, and subsequently find the best way to reach the hikers position. The complete explanation for the searching procedure is long even if not too complex, but based upon qualitative observation and deduction derived from expertise of the rescuer.

Generally speaking, what we need to know is the fact that a simple translation of this procedure in a machine with limited computational power is not practically possible.

A comprehensive description of the companion search and Mountain Rescue procedure could be found in [21].

1.4 Autonomous VTOL for buried searching

The thesis is built around the main thread of inspect and derive the avionics of an autonomous VTOL. Even if avionics refer to the complete set of instrumentation and algorithms necessary to stabilize and control the flight, in this work we will focus on some of the main aspects necessary to perform the main task of buried searching.

This work is not the first attempt to bring an automatic drone on avalanches. Some remarkable examples are

- SHERPA, European project born to create a robotic framework of helpers for Mountain Rescue, coordinated by University of Bologna
- An user-piloted quad-copter research is just started in Politecnico di Torino
- the project Alcedo from the Eidgenössische Technische Hochschule Zürich⁶

⁶ Luc Oth Manuel Grauwiler. Fully autonomous search for avalanche victims using an mav, 2010

1.4.1 Why the use of a VTOL?

The use of a drone in the searching area depends on various factors. During design it is necessary to understand and think a system the fit entirely the actual search strategy.

One practical example of use could be a situation of high residual danger and an uncertainty about the presence of buried under the avalanche. In a case like that, the VTOL could be used to test the necessity of drop the rescue team on the avalanche.

The main advantage is obviously the ability to move faster on the avalanche with respect to an human rescuer, avoiding ground difficulties. At the same time, the drone should be able to identify and avoid obstacle like trees and ski-lift pillars.

1.4.2 Quality Function Deployment

⁷ Mizuno Shigeru Akao Yoji. *QFD: The customer-driven approach to quality planning and deployment*. Asian Productivity Organization, Tokio, J, 1994

The best way to define the characteristics of a new product is to inspect customer needs, and from qualitative user domain extrapolate quantitative engineering dimensions⁷.

Customer Needs

From our interviews of Mountain Rescue members, we have derived some conclusions:

- one of the main cause of an avalanche is the weather, that modifies snow characteristics; during one day multiple avalanches may fall, so it is fundamental to guarantee a long, even if discontinue, operative time
- the VTOL should be portable, with limited size and weight, but at the same time ready to be used in a short amount of time
- all design process should take in to account the extreme low temperature and the high altitude (lower air density)
- ARTVA device on the drone has to be robust with respect to electromagnetic interferences (propeller engines, radio, ...)
- user interface is simple while complete
- the marking of the victims shall be hardware, with the use of visible darts

We are now able to define a table 1.1 in which at each customer needs a rating is given.

In future, the automatic recognition of the avalanche dimensions could be a good starting point for some advanced research in the field of computer vision, or the improvements of user interface using voice recognition over radio.

Customer Need	Rating
Identifies buried person	5
Is autonomous	5
Returns to rescuer position	5
Searches for the signall	5
Is fast	5
Marks physically buried position	5
Operates at avalanche temperatures	5
Performs more than one operation during the day	3
Is usable by anyone	3
Is robust with respect to EM interferences	5
Is portable in a 35L bag	3
Is quiet	2
Is compatible with other rescue vehicles	5
Disengages from the winch	5
Respects ENAC normatives	3

Table 1.1: Customer needs

Technical Specification

The next step in the definition of a good design is a list of technical specifications that will help us to identify the most challenging problems in and the gravity of those problems with respect to the costumer needs.

For sure, one of the first and most challenging complication is the weight reduction, that guarantees a longer flying time. Also those elements are related to the number of propulsion vector and the main dimension (the length of the arm). It is evident the correlation between the number of lift vectors with respect to the maximum wind interference.

For the definition of a good searching algorithm, as we will see, it is important a good resolution of position and attitude of the drone; while to avoid obstacle it is important the resolution and the maximum revealing distance of the range finders.

One final aspect that should be considered are the data related to the system that performs the marking of a buried person.

All the specifications are listed in table 1.2

Merging the tables and comparison

In table 1.4 all data are compared with a weighting method. The table shows the comparison between technical specifications and customer needs and also between technical specifications and the other technical specifications.

Components selection

From the merged data it was possible to select the components that will be used in the prototype. All components are listed in table 1.3

We have also decided not to use a commercial ARTVA, but instead try to build a digital one from scratch. This will allow us to get a lighter model, and also extract exactly the information that we want from the received signal. Even if some device have a serial port, the output data are filtered with models that incorporate the possible speed of a rescue, that is different from our VTOL.

Technical Spec.	Dim.
Flying time	min
Weight	kg
N. of antennas	
Battery Temperature	°C
Range Ultrasonic RF	m
Arm Length	m
Control TX distance	m
GPS Resolution	m
Lateral Speed	$m s^{-1}$
Wind Speed	$m s^{-1}$
ARTVA RX distance	m
Resolution Ultrasonic RF	m
Lift Force	N
N. Disassembled pieces	
N. Darts	
N. Lift Vector	
Maximum inclination	rad
Operative height	m
IMU Resolution	$m s^{-1}$
Weight Marking Device	kg
Weight Dart	kg
Weight ARTVA	kg

Table 1.2: Technical specifications

N	Component	Description	Price
1×	Autoquad 6 Flight Controller	Imu board and stabilization controller	299.00€
6×	Autoquad ESC32	Electronic speed controller	239.40€
6×	Flyduino HE4108 700kV Out-runner	Motors	299.40€
6×	HQ 12"per 4.5"CW and CCW Carbon propeller	Propeller	73.80€
2×	SLS Xtron 5000mA h 14.8V	Batteries	119.98€
3×	USB UART Adapter	Bridge between USB and device UART	9.90€
		Total	1041.48€

Table 1.3: Components list

Legend:

Cust. needs vs. Tech. spec.:

- no relation
 - light relation
 - strong relation

Tech. spec. vs. Tech. spec.:

 - ▼ negative strong relation
 - ▽ negative light relation
 - no relation
 - △ positive light relation
 - ▲ positive strong relation

Table 1.4: Comparison Table

2

Design of a digital ARTVA

Contents

2.1	Analysis of transmitting pattern	22
2.1.1	Maxwell's Equations	22
2.1.2	EM field dynamic potentials	22
2.1.3	Magnetic dipole radiation	24
<i>Potential of a magnetic dipole</i>	24	
<i>Electric and magnetic field</i>	25	
2.1.4	Magnetic field model simplification	25
<i>Re-definition in complex domain</i>	27	
<i>From Polar to Cartesian coordinates</i>	27	
2.2	Analytical signal analysis - A₁-A	28
2.3	Receiving antenna	29
2.3.1	Coils receiver	29
<i>Single coil receiver</i>	29	
<i>Ferrite effect</i>	29	
<i>Antenna effective height</i>	30	
2.3.2	Equivalent circuit and noise	31
<i>Signal</i>	31	
<i>Noise</i>	31	
2.4	Digital ARTVA prototype	32
2.4.1	Tuned tank	33
2.4.2	Buffer and pre-amplification	33
2.4.3	Identification	34
2.4.4	Amplifier	35
2.4.5	Digital stage	35
2.4.6	Dual supply	35
2.4.7	Tri-axes ARTVA	36
2.5	Appendix	38
2.5.1	Polar coordinates	38
2.5.2	Evidences	38
<i>EM field dynamic potential</i>	38	
<i>Magnetic dipole radiation</i>	39	
<i>Complex version of magnetic field</i>	40	
<i>The field in cartesian coordinates</i>	41	
2.5.3	Antenna transfer function	42

In this chapter we will try to design a digital receiver for the ARTVA signal. Before starting with the design, *ARTVA signal* is deeply analyzed, with the derivation of a simplified model for a field pattern that could be used for the implementation of the searching algorithm. After that, ferrite antennas are studied, as they are the only way to receive such a long wavelength. In the last part of the chapter the circuitry for the ARTVA receiver is shown and explained.

2.1 Analysis of transmitting pattern

A formal model of the transmitting pattern is fundamental for the implementation of the searching algorithm. We start from the basic Maxwell's equation and we arrive to a simpler model numerically usable.

As we will see, radiating pattern is quite complex due to the fact that we are working in the **near-field** region, condition that constraint us to not use classical DoA, such as MUSIC or ESPRIT, that operates in far-field condition and at higher frequencies. DoA systems for long waves usually requires too big electro-mechanical devices.

DoA: Direction of Arrival

2.1.1 Maxwell's Equations

The following investigation is based upon Maxwell's Equation, in which the magnetic permeability μ and dielectric constant ϵ are considered constant (the radiation is assumed to propagate at speed of light in air). Also we consider some field properties, that are function of radio distance \mathbf{r} and time t :

$$f(\mathbf{r}, t) = f \quad f \in [\rho, \mathbf{J}, \mathbf{E}, \mathbf{B}, \mathbf{H}]$$

The equations that rule the induction are the *Gauss equation of magnetic induction* and the *Faraday law of electric induction*:

$$\nabla \cdot \mathbf{B} = 0 \tag{2.1}$$

$$\nabla \times \mathbf{E} = -\frac{\partial}{\partial t} \mathbf{B} \tag{2.2}$$

while the equations that rule the interaction with materials are *Gauss equation* and *Ampere law*:

$$\nabla \cdot \mathbf{E} = \frac{\rho}{\epsilon_0} \tag{2.3}$$

$$\nabla \times \mathbf{B} = \mu_0 \left(\mathbf{J} + \epsilon_0 \frac{\partial}{\partial t} \mathbf{E} \right) \tag{2.4}$$

2.1.2 EM field dynamic potentials

Starting from equation 2.1, we can define a vectorial function called *potential vector A* of \mathbf{B} :

$$\mathbf{B} = \nabla \times \mathbf{A} \tag{2.5}$$

We insert 2.5 in 2.2:

$$\nabla \times \mathbf{E} = -\frac{\partial}{\partial t} (\nabla \times \mathbf{A})$$

$$\nabla \times \left(\mathbf{E} + \frac{\partial \mathbf{A}}{\partial t} \right) = 0 \quad (2.6)$$

From the previous equation it is evident that the argument between parentheses is in reality an irrotational vector field, thus a potential function exists such that:

$$-\nabla \phi = \mathbf{E} + \frac{\partial \mathbf{A}}{\partial t}$$

and we derive the following definition of electric field:

$$\mathbf{E} = -\nabla \phi - \frac{\partial \mathbf{A}}{\partial t} \quad (2.7)$$

Equation 2.5 and 2.7 are used to express a new formulation for the Maxwell's equation based upon vector potential¹:

¹ The proof is in chapter appendix 2.41

$$\begin{aligned} \nabla^2 \phi + \frac{\partial}{\partial t} \nabla \cdot \mathbf{A} &= -\frac{\rho}{\epsilon_0} \\ \nabla^2 \mathbf{A} - \frac{1}{c^2} \frac{\partial^2 \mathbf{A}}{\partial t^2} - \nabla \left(\nabla \cdot \mathbf{A} + \frac{1}{c^2} \frac{\partial \phi}{\partial t} \right) &= -\mu_0 \mathbf{J} \end{aligned} \quad (2.8)$$

Those equation, even if complex, could be resolved with a well posed boundaries condition problem. Equation are coupled with the current formulation, but could be decoupled using the **Gauge transformation**, also called **recalibration map**, that is in the form:

$$\begin{cases} \mathbf{A}' \mapsto \mathbf{A} + \nabla \psi \\ \phi' \mapsto \phi - \frac{\partial \psi}{\partial t} \end{cases} \quad (2.9)$$

in which $\psi = \psi(\mathbf{r}, t) \in C^2$. As proofed in 2.42, this map represents an invariant with respect to dynamic potential formulation. If we consider a ψ such that it verifies the **Lorentz equation**

$$\nabla \cdot \mathbf{A}' = -\frac{1}{c^2} \frac{\partial \phi'}{\partial t} \quad (2.10)$$

we obtain in the previous equations the decoupled version:

$$\begin{aligned} \nabla^2 \phi - \frac{1}{c^2} \frac{\partial^2 \phi}{\partial t^2} &= -\frac{\rho}{\epsilon_0} \\ \nabla^2 \mathbf{A} - \frac{1}{c^2} \frac{\partial^2 \mathbf{A}}{\partial t^2} &= -\mu_0 \mathbf{J} \end{aligned} \quad (2.11)$$

Those dynamic equations describe the time evolution of an EM-field. If field sources are located in a finite region, those equations admit as solution a generalization of the well know solution of stationary case, called retarded potential:

$$\begin{aligned} \phi(\mathbf{r}, t) &= \frac{1}{4\pi\epsilon_0} \iiint_{\Omega} \frac{1}{|\mathbf{r} - \mathbf{r}'|} \rho \left(\mathbf{r}', t - \frac{|\mathbf{r} - \mathbf{r}'|}{c} \right) d\mathbf{r} \\ \mathbf{A}(\mathbf{r}, t) &= \frac{\mu_0}{4\pi} \iiint_{\Omega} \frac{1}{|\mathbf{r} - \mathbf{r}'|} \mathbf{J} \left(\mathbf{r}', t - \frac{|\mathbf{r} - \mathbf{r}'|}{c} \right) d\mathbf{r} \end{aligned} \quad (2.12)$$

The existence of \mathbf{A} is verified by property of ∇ operator, whom states that the divergence of a curl of a vector field is zero

in which the vector distance $\mathbf{r} - \mathbf{r}'$ is the distance between the point where retarded potential is evaluated and the point where the element of volume $d\mathbf{r}$ of the localized sources is located. The delay is due to the definition of time:

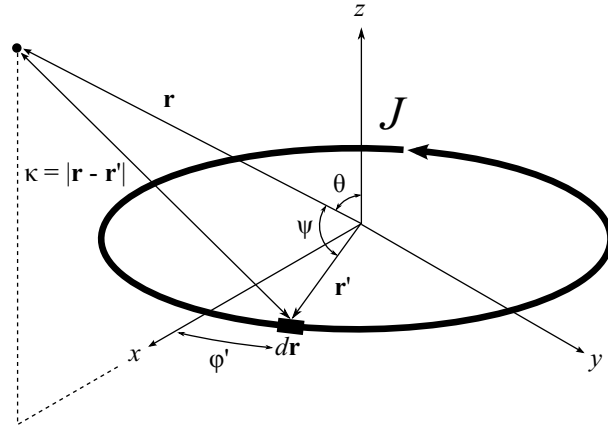
$$t_r = t - \frac{|\mathbf{r} - \mathbf{r}'|}{c}$$

2.1.3 Magnetic dipole radiation

Potential of a magnetic dipole

Our antenna may be seen as an ideal magnetic dipole. The

Figure 2.1: Formulation of magnetic dipole problem



transmitting antenna is a solenoid with a ferrite core, that acts as source of the electro-magnetic field. The source is subject to a dipole magnetic moment induced by the current $J = J_0 \cos(\omega_0 t)$, with no free charges (null scalar potential). The magnetic dipole moment is:

$$\mathbf{m} = \pi r'^2 J \hat{\mathbf{z}} = m_0 \cos(\omega_0 t) \hat{\mathbf{z}} \quad (2.13)$$

From figure 2.1 we define the retarded potential equation, with $\kappa = |\mathbf{r} - \mathbf{r}'|$:

$$\mathbf{A}(\mathbf{r}, t) = \frac{\mu_0}{4\pi} \int \frac{J_0 \cos(\omega_0(t - \kappa/c))}{r} \cos(\varphi') d\varphi' \hat{\phi}$$

In the hypothesis of $\mathbf{r} \parallel \hat{\mathbf{z}} \times \hat{\mathbf{x}}$, we obtain a vector \mathbf{A} directed along $\hat{\mathbf{y}}$:

$$\mathbf{r} = r \sin(\theta) \hat{\mathbf{x}} + r \cos(\theta) \hat{\mathbf{z}}$$

$$\mathbf{r}' = r' \cos(\varphi') \hat{\mathbf{x}} + r' \sin(\varphi') \hat{\mathbf{y}}$$

$$\kappa = \sqrt{(\mathbf{r} - \mathbf{r}') \cdot (\mathbf{r} - \mathbf{r}')}}$$

Those elements in retarded potential formulation lead us to the integral formulation that has only one angular dependency:

$$\mathbf{A}(\mathbf{r}, t) = \frac{\mu_0 J_0 r'}{4\pi} \int_0^{2\pi} \frac{\cos(\omega_0(t - \kappa/c))}{\kappa} \cos(\varphi') d\varphi' \hat{\phi} \quad (2.14)$$

The solution of this integral is reported in appendix; we recall only the simplification used:

- we assume $r' \ll r$
- we assume $r' \ll \lambda = 2\pi c/\omega_0$

that brings us to the following solution:

$$\mathbf{A}(\mathbf{r}, t) = \frac{\mu_0 m_0}{4\pi r} \sin(\theta) \left(\frac{1}{r} \sin(\omega_0(t - r/c)) - \frac{\omega_0}{r} \cos(\omega_0(t - r/c)) \right) \hat{\phi} \quad (2.15)$$

in which m_0 identifies the total dipole moment, considering also the number of the coils of antenna. The rest of the equation describes the propagation of the transmission in near-field conditions.

Electric and magnetic field

With null scalar potential we obtain the electric field and the magnetic field from the equations:

$$\begin{aligned} \mathbf{E} &= -\frac{\partial \mathbf{A}}{\partial t} \\ \mathbf{B} &= \nabla \times \mathbf{A} \end{aligned} \quad (2.16)$$

The application of differential operator ∇ :

$$\mathbf{E} = \begin{bmatrix} 0 \\ 0 \\ \frac{\partial A_\phi}{\partial t} \end{bmatrix} \quad \mathbf{B} = \begin{bmatrix} \frac{1}{r} \frac{\partial A_\phi}{\partial \theta} \\ -\frac{\partial A_\phi}{\partial r} \\ 0 \end{bmatrix} \quad (2.17)$$

In polar coordinates:

$$\nabla = \begin{bmatrix} \frac{\partial}{\partial r} \\ \frac{1}{r} \frac{\partial}{\partial \theta} \\ \frac{1}{r \sin(\theta)} \frac{\partial}{\partial \phi} \end{bmatrix}$$

The final formulation for th EM field of a magnetic dipole is:

$$\begin{aligned} \tau &= t - \frac{r}{c} \\ E_\phi &= \frac{\mu_0 m_0}{4\pi} \sin(\theta) \left(\frac{\omega_0}{r^2} \sin(\omega_0 \tau) + \frac{\omega_0^2}{c} \cos(\omega_0 \tau) \right) \\ B_r &= \frac{\mu_0 m_0}{2\pi r^2} \cos(\theta) \left(\frac{1}{r} \cos(\omega_0 \tau) + \frac{\omega_0}{c} \sin(\omega_0 \tau) \right) \\ B_\theta &= \frac{\mu_0 m_0}{4\pi r^3 c^2} \sin(\theta) ((c^2 - \omega_0^2 r^2) \cos(\omega_0 \tau) + \omega_0 r c \sin(\omega_0 \tau)) \end{aligned} \quad (2.18)$$

In figure 2.2 are shown some animation referred to the magnetic field defined in the previous equations. The animation are performed using ARTVA typical parameters, even if time is scaled. The equations are parametric with respect to a value, m_0 that is the transmitter magnetic dipole. As we have seen in chapter 1, the real transmitting power of an avalanche beacon is not known, but it shall have the maximum at 10m inside a range. The animations consider an unitary magnetic dipole moment.

2.1.4 Magnetic field model simplification

From animations it is evident that the effect of retarded propagation is almost null inside a radius of 40m from the transmitting source,

Figure 2.2: Graphical animation of the magnetic field \mathbf{B} with retarded potential formulation. Those graph derives directly from the equations 2.18. To see the animations, please use [Adobe Acrobat viewer](#)

that is roughly the maximum distance at which an avalanche beacon receives the signal. This brings us to other simplifications for our model, as we will see in this section. From now on, all the simplifications are performed with the intent to find a model computationally convenient to be used in our algorithms.

Re-definition in complex domain

The next step is to bring equation of magnetic field in complex domain, but keeping in mind that only real part of the equations keeps the physical meaning of the field. The re-definition is based upon Euler relationship and on the definition of wavenumber:

$$e^{j\beta} = \cos(\beta) + j \sin(\beta)$$

$$\kappa = \frac{\omega_0}{c}$$

$$\begin{aligned} B_r &= \frac{1}{2} \frac{\mu_0 m_0}{\pi} \cos(\theta) \left(\frac{1}{r^3} \cos(\omega_0 \tau) - \frac{\kappa}{r^2} \sin(\omega_0 \tau) \right) \\ &= -\frac{1}{2} j \frac{\mu_0 m_0}{\pi} \kappa^3 \cos(\theta) \left(\frac{1}{j^2 r^2 \kappa^2} + \frac{1}{j^3 r^3 \kappa^3} \right) e^{j\omega_0 \tau} \end{aligned} \quad (2.19)$$

$$\begin{aligned} B_\theta &= \frac{1}{4} \frac{\mu_0 m_0}{\pi r^3 c^2} \sin(\theta) ((c^2 - \omega_0^2 r^2) \cos(\omega_0 \tau) - \omega_0 r c \sin(\omega_0 \tau)) \\ &= -\frac{1}{4} j \frac{\mu_0 m_0}{\pi} \kappa^3 \sin(\theta) \left(\frac{1}{j r \kappa} + \frac{1}{j^2 r^2 \kappa^2} + \frac{1}{j^3 r^3 \kappa^3} \right) e^{j\omega_0 \tau} \end{aligned} \quad (2.20)$$

The proof of those relations is in appendix.

From Polar to Cartesian coordinates

The last approximation is related to the nature of the receiver:

- the receiver act as an identifier of the constant quantity of the field, or the magnitude of the oscillating field
- the distance of the receiver is always in a radius that allows us to not consider the effect of retarded potential:

$$\tau = t - \frac{r}{c} \Big|_{r \ll c} \longrightarrow t$$

Under those considerations, and with MacLaurin first order transformation of B_θ , the formulation of magnetic field real part takes the form:

$$\mathbf{B} = \frac{\mu_0}{4\pi r^3} (2m_0 \cos(\theta) \hat{\mathbf{r}} + m_0 \sin(\theta) \hat{\theta}) \quad (2.21)$$

The projection of the field in cartesian coordinates is:

$$\mathbf{B}(\mathbf{r}, \mathbf{m}) = \frac{\mu_0}{4\pi r^5} \begin{bmatrix} 2x^2 - y^2 - z^2 & 3xy & 3xz \\ 3xy & 2y^2 - x^2 - z^2 & 3yz \\ 3xz & 3yz & 2z^2 - x^2 - y^2 \end{bmatrix} \mathbf{m} \quad (2.22)$$

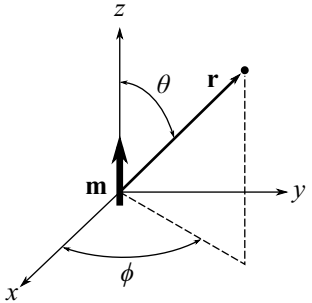


Figure 2.3: From Polar coordinates to Cartesian coordinates

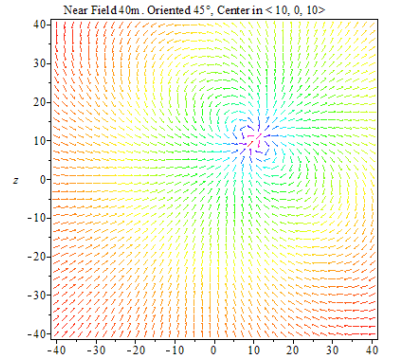


Figure 2.4: Representation of a magnetic field with source:
 $\mathbf{p}_{tx} = [10, 0, 10]^T$
 $\mathbf{m} = [\cos(\pi/4), 0, \sin(\pi/4)]^T$

A final generalization grants us the ability to write a general form of the field that has origin in position different from the origin:

$$\mathbf{B}(\mathbf{p}_{rx} - \mathbf{p}_{tx}, \mathbf{m}) \quad (2.23)$$

That is the form used for our simulations.

2.2 Analytical signal analysis - A1-A

² ETSI EN 300 718-(1 2 3 4). E.r.m. avalanche beacons - transmitter-receiver systems. Technical report, ETSI, 2001

The ARTVA signal is a wild-life tag, specifically an **A-1A** signal. From the normative²:

- **A1A Signal:**
 - amplitude modulated signal
 - digital information (keying)
 - carrier frequency: 457kHz
 - no auxiliary carrier
 - frequency error shall not exceed $\pm 80\text{Hz}$
- **carrier keying characteristics:**
 - on-time: 70ms minimum
 - off-time: 400ms minimum
 - period: $1000\text{ms} \pm 300\text{ms}$
- **H-field peak at 10m**
 - must be greater than $0.5\mu\text{A m}^{-1}$
 - must be lower than $2.23\mu\text{A m}^{-1}$

The variable duty cycle is a challenge for the formulation of a searching algorithm, with a duty cycle (Δ) that varies from a minimum of 5.4% to a maximum of 42.9%. The amplitude modulation, from a mathematical point of view is:

$$J_{tx}(t) = (1 + \mu J_{int}) \cos(\omega_0 t) \quad (2.24)$$

There are 3 key elements:

- J_{int} is the current of the intelligence signal, the representation of the square wave in figure 2.5:

$$J_{int}(t) = A\Delta + \sum_{n=1}^{\infty} \left(\frac{2A}{n\pi} \sin(n\pi\Delta) \cos(\omega_{int}nt) \right) \quad (2.25)$$

in which A represents the signal amplitude and Δ is the duty cycle.

- the frequency of the carrier signal is $f_0 = 2\pi\omega_0$, and it is 457kHz
- μ is called modulation factor

From this current we are able to obtain the magnitude of dipole magnetic vector, using equation 2.13. Many of those parameter are device dependent and not known.

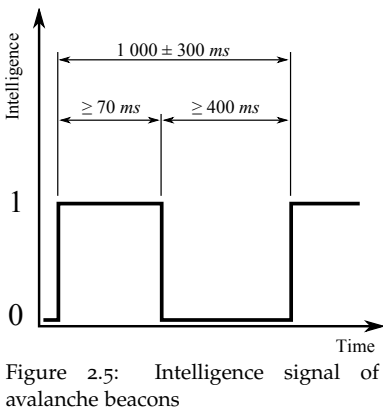


Figure 2.5: Intelligence signal of avalanche beacons

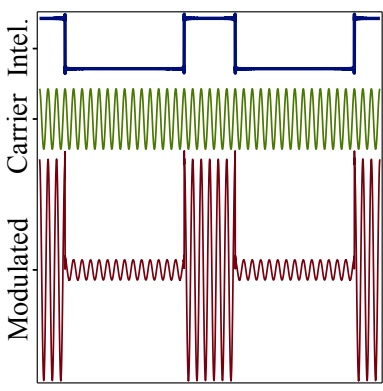


Figure 2.6: Example of a A-1A modulated signal

2.3 Receiving antenna

To receive such a long wavelength with a small dimension device there is almost only one solution: use a ferrite core loop antenna, that is equal to the antenna used for transmission. In the next section, ferrite antenna is analyzed deeply, as a crucial part for the receiver. As we will see from the prototype, obtain a good receiver antenna is a very difficult task, due to the extreme high noise that could be generated by imperfections in windings or material.

2.3.1 Coils receiver

Single coil receiver

Under the hypotheses of an uniform EM field, using Maxwell's equations it is possible to derive potential difference induced in the coil:

$$V_{\text{ind}} = \oint_{\mathcal{C}} \mathbf{E} \cdot d\mathbf{l} = - \frac{d\Phi_B}{dt} \quad (2.26)$$

where flux is:

$$\begin{aligned} \Phi_B &= \int_{A_c} \mathbf{B} \cdot \hat{\mathbf{e}}_a dA \\ &= \mu_0 H A \cos(\theta) \end{aligned} \quad (2.27)$$

It is evident a cosine relation between field and axis of the coil. The value of induced potential is maximum when the magnetic field \mathbf{H} is orthogonal to the coil. θ is the angle between the field and the axis of the coil. Fusing two previous equations, we get:

$$V_{\text{ind}} = \mu_0 A_c \frac{dH}{dt}$$

that for our example:

$$V_{\text{ind}} = -j\omega_0 H A_c \mu_0$$

For conformity with the literature, we express the magnetic field in terms of electric field³:

$$V_{\text{ind}} = \omega_0 N A_c \frac{E}{c} \quad (2.28)$$

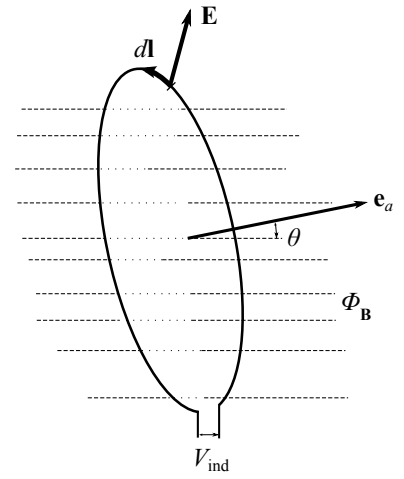


Figure 2.7: Single coil in a field

³ It is known that:

$$\mu_0 H = \frac{E}{c}$$

Ferrite effect

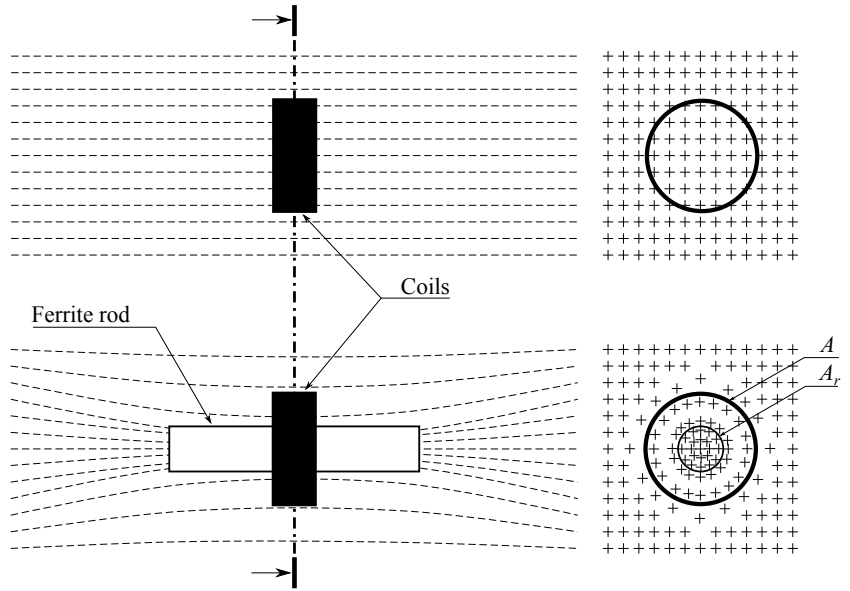
Inserting a ferrite bar brings to a deviation of the magnetic field flux. Fields lines are bended inside the ferrite because of its greater magnetic permeability. The total flux in section A of figure 2.8 is given by the flux that crosses area $A - A_r$ and flux that crosses area A_r :

$$\Phi_T = \Phi_{B_1} + \Phi_{B_2}$$

$$\Phi_{B_1} = \mu_r A_r H$$

$$\Phi_{B_2} = \mu_0 (A - A_r) H$$

Figure 2.8: Flux lines through coil and ferrite rod



and thus the total flux is:

$$\Phi_T = HA_r \left(\mu_r + \mu_0 \left(\frac{A}{A_r} - 1 \right) \right) \quad (2.29)$$

bringing the previous equation in 2.26, and simplifying with respect to constant parts of area, we get:

$$V_{\text{ind}} = \omega_0 N \frac{E}{c} A_r \left(\mu_r + \left(\frac{\phi_c^2}{\phi_r^2} - 1 \right) \right) \quad (2.30)$$

In a real coil, we have a coil diameter that is $\phi_c = \phi'_c + \phi_{\text{wire}}$, and it is usual to approximate $\phi_c \approx \phi_r$, and our antenna equation becomes:

$$V_{\text{ind}} = \omega_0 N \frac{E}{c} A_r \mu_r \quad (2.31)$$

From which appears that the insertion of a ferrite rod in a coils inductance brings to an increase of induced tension proportional to the value of magnetic permeability of the ferrite itself. The identification of this value is not trivial and should be done experimentally. There are only some numerical approximation to the value of μ_0 related to the dimensions of ferrite bar, but it appears evidently a correlation between the ratio bar length/bar diameter. The greater this ratio, the greater the value of permeability⁴.

$$\mu_r \propto \frac{l_r}{\phi_r} \quad (2.32)$$

Antenna effective height

Effective height of antenna is defined as the ratio between the induced potential in the coils end the electric field intensity:

$$h_{\text{eff}} = \frac{V_{\text{ind}}}{E} \quad (2.33)$$

⁴We could give a trivial interpretation to this statement: the greater the length of the ferrite bar, the greater the number of flux lines that are bended into the bar; also the smaller the diameter, the greater the density of bended flux lines, thus the greater the permeability value.

Applying previous equation to the definition of effective height:

$$h_{\text{eff}} = \frac{\omega_0 N A_r}{c} \left(\mu_r + \left(\frac{\phi_c^2}{\phi_r^2} - 1 \right) \right) \quad (2.34)$$

2.3.2 Equivalent circuit and noise

From a pure circuit point of view, ferrite antenna is seen as an RLC circuit, in which we identify three passive components:

- $L \rightarrow \mathbf{Z}_L = j\omega L$: coil inductance
- $R_p \rightarrow \mathbf{Z}_R = R_p$: wire resistance
- $C \rightarrow \mathbf{Z}_C = (j\omega L)^{-1}$: parassite capacitance

The input voltage of the circuit is $V_{\text{ind}} = h_{\text{eff}} E$

Signal

Starting from the definition of the equivalent circuit, with an external resistive load R_L it is possible to derive a transfer function (full derivation in appendix at equation 2.44):

$$\frac{V_{\text{out}}}{V_{\text{ind}}} = G(s) = \frac{\omega_{LC}}{Q_\alpha} \frac{s + Q_\alpha \omega_{LC}}{s^2 + \frac{\omega_{LC}}{Q_\beta} s + \omega_{LC}^2} \quad (2.35)$$

if we obtain an $\omega_{LC} = \omega_0$, we get resonance for an ARTVA incident signal: $s = j\omega_0$:

$$G(j\omega_0) = (-jQ_\beta) \left(1 + \frac{j}{Q_\alpha} \right) \quad (2.36)$$

and then:

$$V_{\text{out}} = h_{\text{eff}} \frac{Q_\beta}{Q_\alpha} E \quad (2.37)$$

Noise

We could consider different sources of noise for our ferrite antenna:

- Boltzmann temperature noise
- ferrite polarization noise
- skin effect noise
- auto-inductance noise
- parasite capacitances due to construction, wirings or circuit grounding

Even if some of those source are easily to model, some of them are not and require an experimental interpolation. For the Boltzmann with the noise:

$$V_{n,B} = \sqrt{4KT\Delta f Q_\beta \mathbf{Z}_L}$$

that is environment dependent. For the other sources, some more considerations must be derived. Skin effect and ferrite noise are proportional to the received field. Those two effects must be carefully taken into account and analyzed from experimental point of view.

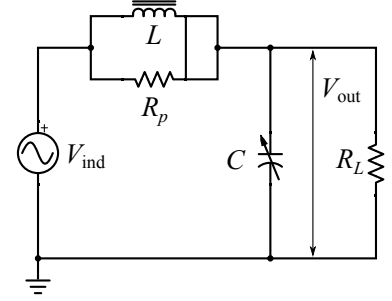


Figure 2.9: Antenna equivalent circuit

$$\begin{aligned} \omega_{LC}^2 &= \frac{1}{LC} \\ Q_\alpha &= \omega_{LC} R_p C \\ Q_\beta &= \omega_{LC} \frac{R_p R_L}{R_p + R_L} C \end{aligned}$$

The first one is due to the distribution of the current in the section of the coil wire: current tends to accumulate in the skin layer of the wire, generating eddy currents that are sources of noise. To this effect, some special woven wire, like litz wire, should be used. The second effect, ferrite noise, derives from the polarization of the magnetic crystal inside ferrite. To polarize the whole ferrite bar, some energy must be spent to move magnetic domain, and the movement of those domain generates a noise. This effect is strictly related to the quality of material and cannot be mitigated. Auto-inductance noise is due to the current that is absorbed by the serial circuit of antenna and load. In a production of a prototype it is important that input of identification circuit has a very high impedance to reduce a generation of this current on antenna. Some high quality devices implement a secondary loop on the antenna that acts as a re-generator, that tries to null those parasitic currents effect.

It is straightforward now, that all those noise effect could be resumed in an unique interpolated expression $n(V_{\text{ind}}, T)$.

For simulation purpose it is possible to simulate this as Gaussian white noise as follows:

$$\sigma = N(\mathbf{0}, V_{n,B}) + 10^x |V_{\text{ind}}| N(\mathbf{0}, \Sigma) \quad (2.38)$$

with x a value that scales the proportional noise.

2.4 Digital ARTVA prototype

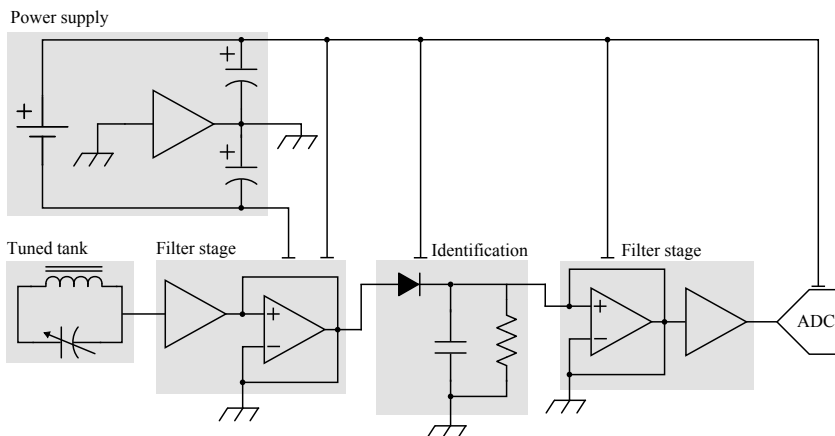


Figure 2.10: Block diagram for the circuit

In the last section of this chapter, we use the knowledge collected to develop a prototype of an ARTVA receiver, in which there is not a transmission part. The receiver is the only fundamental module that we need for our drone, a transmitter will only be useless weight.

In figure 2.10 there is the block outline of the device:

- the first block is the tuned tank, or tuned amplifier
- the second block is the buffer and pre-amplifier
- the third block is the identification part

- an amplification and a second buffer
- digital component
- dual supply stage

Through this section, each block will be discussed and explained. The design process has taken into account the tolerances for passive components⁵, but nothing can be done for thermal derive, that increases tolerance ranges to almost unpredictable values.

⁵ Resistors: 5%
Capacitors: 20%

2.4.1 Tuned tank

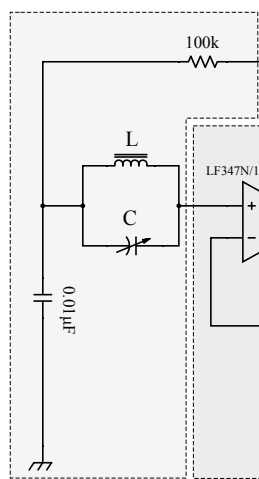


Figure 2.11: Tuned tank portion of circuit

The tuned tank is composed by a ferrite antenna, with a rod of 10cm per \varnothing 1cm. The wire of the coil is a 30 AWG enameled copper wire, with a final parasite resistance of 22Ω . The coil has 70 windings. For more informations about this tuned circuit, check previous section.

2.4.2 Buffer and pre-amplification

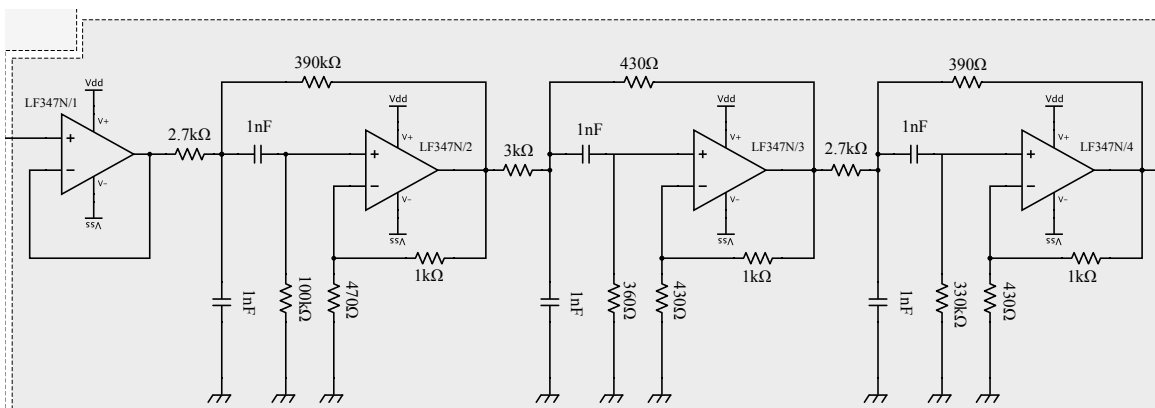


Figure 2.12: Pre-amplifier stage

This block is composed by a first stage that acts as a separation between the tuned tank and the filter, also called voltage follower. To limit the number of components on the board this stage is obtained with an operational amplifier. To grant a longer receiving range, an

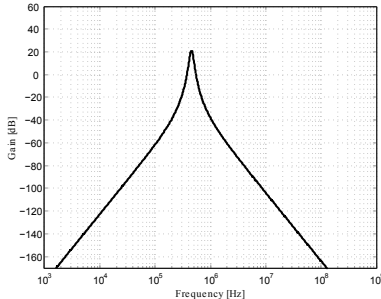


Figure 2.13: Filter magnitude characteristic

high-gain selective active filter is in cascade to the buffer before the identification and acts as a pre-amplifier. It is important to select an operational amplifier with an high bandwidth-gain-product to grant the gain at 457kHz, at which the filter is centered. Also, this stage depends to the dual $\pm 5V$ supply stage.

The op-amp chosen is LF347N, even if a faster amplifier may be selected, it is advised to stay below the 60MHz BW, to avoid auto-resonance effects.

2.4.3 Identification

Figure 2.14: Identification stage

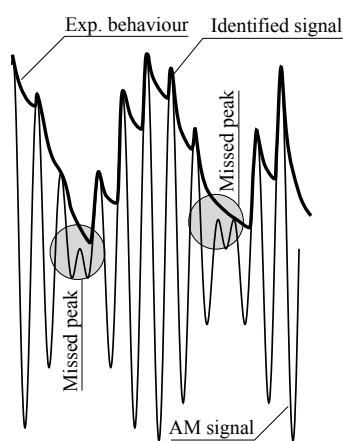
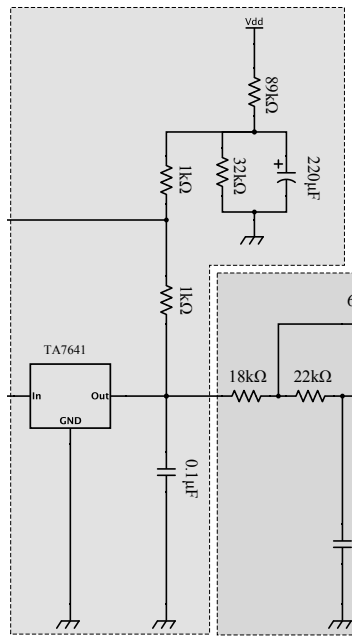


Figure 2.15: Logical function of an identifier

⁶ A.k.a.: MK484 evolution of ZN414



The central block is an identification circuit, obtained with the monolithic classical IC TA7641⁶, that acts as a one chip radio solution in AM. All receiver is derived from the modification of the basic circuit provided in schematics of this IC, extended with filtering and buffers, and the removal of the auto gain control resistance in the output feedback. Also, transistor amplification stage is removed. The output of this circuitry is in 40 to 60mV, with a very low current required. The input pin has a good impedance

To better understand the use of this stage, look at figure 2.15, in which an extremely simplified version of the IC behavior is represented with common components that are drawn in figure 2.10. The IC straightens the received signal and identifies the envelope of the modulated intelligence with a low pass filter that has a dynamic not too slow, to not loose some of the higher frequencies information modulated (also called missed peak). IC implements this function with an high quality envelope detector.

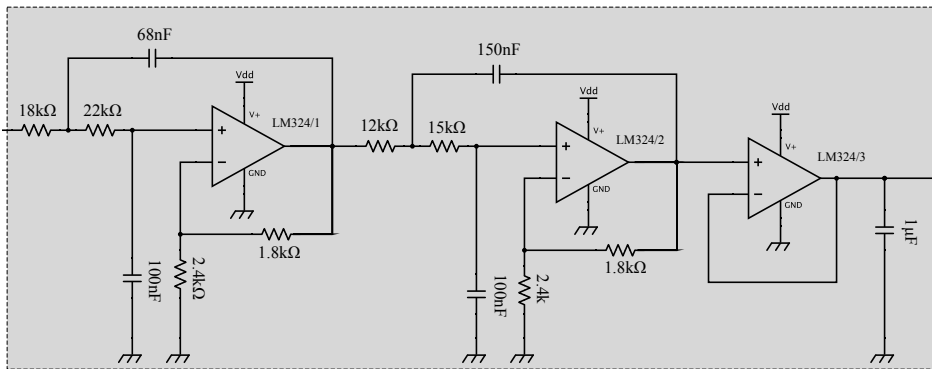


Figure 2.16: Low pass filter and amplification stage

2.4.4 Amplifier

The identified signal is, again, amplified and filtered, to a lower frequency, to grant the isolation of the square wave, with respect to the residual carrier and other source of interference. A 10dB gain filter, with 2 stages was implemented. After the filter, another buffer connects analog circuitry with digital micro-controller.

2.4.5 Digital stage

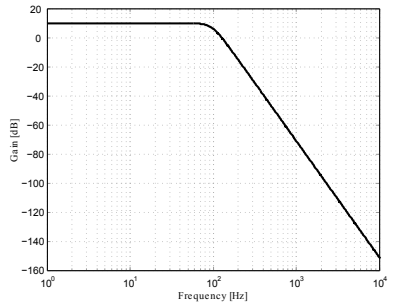
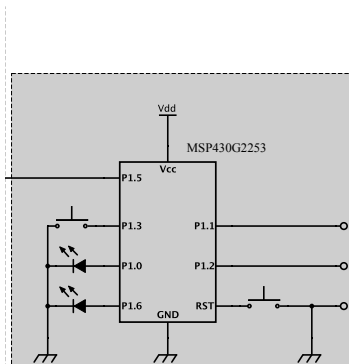


Figure 2.17: Filter magnitude characteristic

Figure 2.18: Digital stage

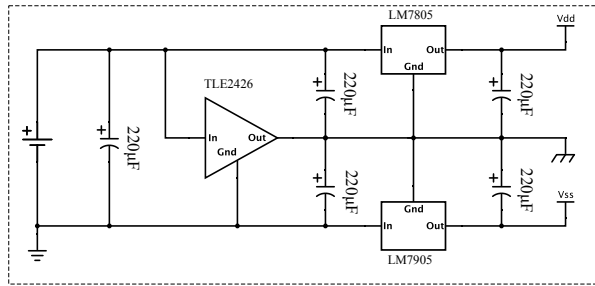


One last stage is the ADC and the UART interface on the microcontroller. Using an MSP430 it is easy to develop in C the routines necessary to perform the task. To reduce the power consumption, ADC sampling is performed with ALU in power saving mode. Once the sampling task is completed, an interrupt brings up the ALU that set up the variables too be sent over serial interface UART (or SPI or I₂C).

2.4.6 Dual supply

The supply is obtained through the use of a virtual ground and a symmetrical classical regulation circuit. This scheme is sometimes called rail splitter, and it is necessary for the first regulation stage, to avoid op-amps saturation.

Figure 2.19: Example of a sampling result



2.4.7 Tri-axes ARTVA

In figure 2.19 there is an example of sampling from the real prototype, using MATLAB serial reading capabilities. A complete prototype uses three equal antenna–filter–identification–amplifier stage, with orthogonal antennas, and one single ADC micro–controller and power supply unit.

Figure 2.20: Complete circuit

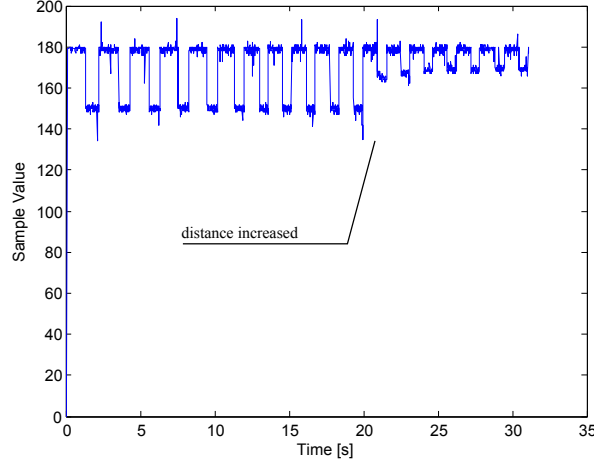


Figure 2.21: Triple antenna

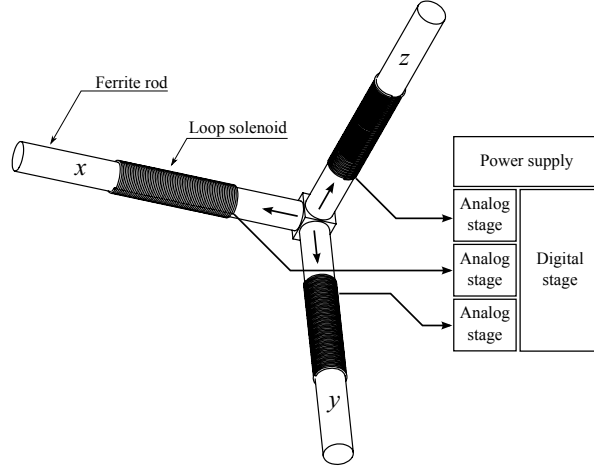
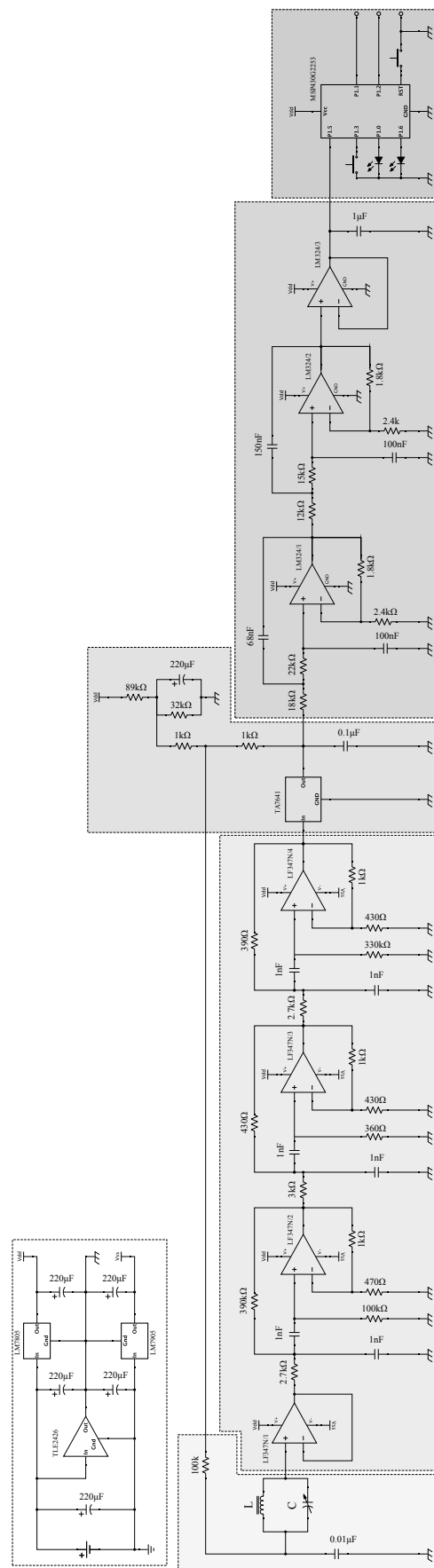


Figure 2.22: Complete circuit



2.5 Appendix

2.5.1 Polar coordinates

Maps:

$$\begin{cases} x = r \sin(\theta) \cos(\phi) \\ y = r \sin(\theta) \sin(\phi) \\ z = r \cos(\theta) \end{cases} \rightarrow \begin{cases} r = \sqrt{x^2 + y^2 + z^2} \\ \theta = \arctan\left(\frac{z}{\sqrt{x^2 + y^2}}\right) \\ \phi = \arctan\left(\frac{x}{y}\right) \end{cases} \quad (2.39)$$

Vectors in Cartesian coordinates:

$$\begin{bmatrix} \hat{\mathbf{r}} & \hat{\theta} & \hat{\phi} \end{bmatrix} = \frac{1}{\sqrt{x^2 + y^2 + z^2}} \begin{bmatrix} x & \frac{xz}{\sqrt{x^2 + y^2}} & -\frac{y}{\sqrt{x^2 + y^2}} \\ y & -\frac{yz}{\sqrt{x^2 + y^2}} & \frac{x}{\sqrt{x^2 + y^2}} \\ z & -\frac{x^2 + y^2}{\sqrt{x^2 + y^2}} & 0 \end{bmatrix} \quad (2.40)$$

2.5.2 Evidences

EM field dynamic potential

The following equations are the proof for 2.8

$$\begin{aligned} \nabla \cdot \left(-\nabla \phi - \frac{\partial \mathbf{A}}{\partial t} \right) &= \frac{\rho}{\epsilon_0} \\ \nabla^2 \phi + \frac{\partial}{\partial t} \nabla \cdot \mathbf{A} &= -\frac{\rho}{\epsilon_0} \end{aligned}$$

$$\begin{aligned} \mu_0 \left(\mathbf{J} + \epsilon_0 \frac{\partial}{\partial t} \left(-\nabla \phi - \frac{\partial \mathbf{A}}{\partial t} \right) \right) &= \nabla \times (\nabla \times \mathbf{A}) \\ \mu_0 \mathbf{J} - \mu_0 \epsilon_0 \frac{\partial^2 \mathbf{A}}{\partial t^2} - \mu_0 \epsilon_0 \nabla \frac{\partial \phi}{\partial t} &= \nabla (\nabla \cdot \mathbf{A}) - \nabla^2 \mathbf{A} \\ \nabla^2 \mathbf{A} - \frac{1}{c^2} \frac{\partial^2 \mathbf{A}}{\partial t^2} - \nabla \left(\nabla \cdot \mathbf{A} + \frac{1}{c^2} \frac{\partial \phi}{\partial t} \right) &= -\mu_0 \mathbf{J} \end{aligned} \quad (2.41)$$

In the following equation invariance with respect to recalibration

map is showed:

$$\begin{aligned}
 \nabla \times \mathbf{A}' &= \nabla(\mathbf{A} + \nabla\psi) \\
 &= \nabla \times \mathbf{A} + \nabla \times \nabla\psi \\
 &= \nabla \times \mathbf{A} \\
 &= \mathbf{B}
 \end{aligned} \tag{2.42}$$

$$\begin{aligned}
 -\nabla\phi' - \frac{\partial \mathbf{A}'}{\partial t} &= -\nabla\left(\phi - \frac{\partial\psi}{\partial t}\right) - \frac{\partial}{\partial t}(\mathbf{A} + \nabla\psi) \\
 &= -\nabla\phi + \nabla\frac{\partial}{\partial t}\psi - \frac{\partial\mathbf{A}}{\partial t} - \frac{\partial}{\partial t}\nabla\psi \\
 &= -\nabla\phi - \frac{\partial\mathbf{A}}{\partial t} \\
 &= \mathbf{E}
 \end{aligned}$$

Magnetic dipole radiation

To evaluate the integral 2.14 we should consider some simplifications.

$r' \ll r$: for an ideal dipole, coils radius shall be really with respect to radio vector:

$$\begin{aligned}
 \kappa &= \sqrt{(\mathbf{r} - \mathbf{r}') \cdot (\mathbf{r} - \mathbf{r}')} = \\
 &= \sqrt{\mathbf{r} \cdot \mathbf{r} + \mathbf{r}' \cdot \mathbf{r}' - 2 \mathbf{r} \cdot \mathbf{r}'} \\
 &= \sqrt{r^2 + r'^2 - 2rr' \sin(\theta)\cos(\varphi')} \\
 &= r \sqrt{1 + \frac{r'^2}{r^2} - 2 \frac{r'}{r} \sin(\theta)\cos(\varphi')}
 \end{aligned}$$

the simplification is performed by the use of Taylor expansions, under the hypothesis of $r'^2/r^2 \approx 0$:

$$\begin{aligned}
 \kappa &= \text{Taylor}_2 \left[r \sqrt{1 - 2 \frac{r'}{r} \sin(\theta)\cos(\varphi')} \right]_{\frac{r'}{r} \rightarrow 0} \\
 &\approx r \left(1 - \frac{r'}{r} \sin(\theta)\cos(\varphi') \right)
 \end{aligned}$$

imposing the inverse:

$$\begin{aligned}
 \frac{1}{\kappa} &= \frac{1}{r} \left(1 - \frac{r'}{r} \sin(\theta)\cos(\varphi') \right)^{-1} \\
 &= \text{Taylor}_2 \left[\frac{1}{r} \left(1 - \frac{r'}{r} \sin(\theta)\cos(\varphi') \right)^{-1} \right]_{\frac{r'}{r} \rightarrow 0} \\
 &\approx \frac{1}{r} \left(1 - \frac{r'}{r} \sin(\theta)\cos(\varphi') \right)^{-1}
 \end{aligned}$$

$r' \ll \lambda = 2\pi c/\omega_0$: this observation permits us to simplify the cosine in the argument of the integral, with τ as defined in 2.18:

$$\begin{aligned}
 \cos(\gamma + \beta) &= \cos\gamma \cos\beta - \sin\gamma \sin\beta \\
 \text{for } \gamma \rightarrow 0 \text{ we get } \sin(\gamma) &\approx \omega_0\tau \text{ and} \\
 \cos(\gamma) &\approx 1
 \end{aligned}$$

$$\begin{aligned}
\cos \left(\omega_0 \left(t - \frac{\kappa}{c} \right) \right) &\approx \cos(\omega_0 \tau) + \frac{\omega_0 r'}{c} \sin(\theta) \cos(\varphi') \\
&= \cos(\omega_0 \tau) \cos \left(\frac{\omega_0 r'}{c} \sin(\theta) \cos(\varphi') \right) - \\
&\quad + \sin(\omega_0 \tau) \sin \left(\frac{\omega_0 r'}{c} \sin(\theta) \cos(\varphi') \right) \\
&\approx \cos(\omega_0 \tau) - \\
&\quad + \sin(\omega_0 \tau) \sin \left(\frac{\omega_0 r'}{c} \sin(\theta) \cos(\varphi') \right)
\end{aligned}$$

The union of the two simplifications give us as integral argument:

$$\begin{aligned}
&\frac{1}{r} \left(1 + \frac{r' \cos(\theta) \sin(\varphi')}{r} \right) \cdot \\
&\cdot \left(\cos(\omega_0 \tau) - \frac{\omega_0 r' \sin(\theta) \cos(\varphi') \sin(\omega_0 \tau)}{c} \right)
\end{aligned}$$

expanding and considering $\xi = \sin(\theta) \cos(\varphi')$ we obtain:

$$\frac{1}{r} \left(\frac{\omega_0 \sin(\omega_0 \tau) \xi r'}{c} + \cos(\omega_0 \tau) - \frac{\omega_0 \sin(\omega_0 \tau) \xi r'^2}{cr} + \frac{\cos(\omega_0 \tau) \xi r'}{r} \right)$$

where the term $\frac{r'^2}{cr} = \frac{r'}{r} \frac{\omega_0}{2\pi} \frac{r'}{\lambda} \approx 0$ as we have already stated:

$$\frac{1}{r} \left(\cos(\omega_0 \tau) - \left(\frac{\omega_0}{c} \sin(\omega_0 \tau) - \frac{1}{r} \cos(\omega_0 \tau) \right) r' \xi \right)$$

extracting only the parts that are function of integration variable φ' :

$$\begin{aligned}
a_1 &= \frac{1}{r} \cos(\omega_0 \tau) \\
a_2 &= \frac{1}{r} \left(\frac{\omega_0}{c} \sin(\omega_0 \tau) - \frac{1}{r} \cos(\omega_0 \tau) \right) r' \sin(\theta)
\end{aligned}$$

The final integral is in the form:

$$\mathbf{A}(\mathbf{r}, t) = \frac{\mu_0 J_0 r'}{4\pi r} \int_0^{2\pi} a_1 \cos(\varphi') - a_2 \cos^2(\varphi') d\varphi' \hat{\phi}$$

$$\int_0^{2\pi} \cos(\varphi') d\varphi' = 0$$

$$\int_0^{2\pi} \cos^2(\varphi') d\varphi' = \pi$$

and thus solved:

$$\begin{aligned}
\mathbf{A}(\mathbf{r}, t) &= -\frac{\mu_0 J_0 r'}{4\pi} \pi a_2 \\
&= \frac{\mu_0 J_0 r'^2 \pi}{4\pi r} \left(\frac{1}{r} \cos(\omega_0 \tau) - \frac{\omega_0}{c} \sin(\omega_0 \tau) \right)
\end{aligned}$$

Applying the substitution $m_0 = \pi r'^2 J_0$ we found the solution reported in equation 2.15.

Complex version of magnetic field

Here the proof of complex magnetic field equations:

$$\begin{aligned}
 B_r &= \frac{1}{2} \frac{\mu_0 m_0}{\pi} \cos(\theta) \left(\frac{1}{r^3} \cos(\omega_0 \tau) - \frac{\kappa}{r^2} \sin(\omega_0 \tau) \right) \\
 &= \frac{1}{2} \frac{\mu_0 m_0}{\pi} \cos(\theta) \kappa^3 \left(\frac{1}{r^3 \kappa^3} \cos(\omega_0 \tau) - \frac{1}{r^2 \kappa^2} \sin(\omega_0 \tau) \right) \\
 &= \frac{1}{2} \frac{\mu_0 m_0}{\pi} \cos(\theta) \kappa^3 \left(\frac{1}{r^3 \kappa^3} + \frac{j}{r^2 \kappa^2} \right) e^{j\omega_0 \tau} \\
 &= \frac{1}{2} \frac{\mu_0 m_0}{\pi} \cos(\theta) \kappa^3 \left(\frac{j}{r^2 \kappa^2} + \frac{1}{r^3 \kappa^3} \right) e^{j\omega_0 \tau} \\
 &= -\frac{1}{2} j \frac{\mu_0 m_0}{\pi} \kappa^3 \cos(\theta) \left(\frac{1}{j^2 r^2 \kappa^2} + \frac{1}{j^3 r^3 \kappa^3} \right) e^{j\omega_0 \tau}
 \end{aligned}$$

$$\begin{aligned}
 B_\theta &= \frac{1}{4} \frac{\mu_0 m_0}{\pi r^3 c^2} \sin(\theta) ((c^2 - \omega_0^2 r^2) \cos(\omega_0 \tau) - \omega_0 r c \sin(\omega_0 \tau)) \\
 &= \frac{1}{4} \frac{\mu_0 m_0}{\pi} \sin(\theta) \left(\left(\frac{1}{r^3} - \frac{\omega_0^2}{c^2 r} \right) \cos(\omega_0 \tau) - \frac{\omega_0}{r^2 c} \sin(\omega_0 \tau) \right) \\
 &= \frac{1}{4} \frac{\mu_0 m_0}{\pi} \sin(\theta) \left(\left(\frac{1}{r^3} - \frac{\kappa^2}{r} \right) \cos(\omega_0 \tau) - \frac{\kappa}{r^2} \sin(\omega_0 \tau) \right) \\
 &= \frac{1}{4} \frac{\mu_0 m_0}{\pi} \sin(\theta) \kappa^3 \left(\left(\frac{1}{r^3 \kappa^3} - \frac{1}{r \kappa} \right) \cos(\omega_0 \tau) - \frac{1}{r^2 \kappa^2} \sin(\omega_0 \tau) \right) \\
 &= \frac{1}{4} \frac{\mu_0 m_0}{\pi} \sin(\theta) \kappa^3 \left(\left(\frac{1}{r^3 \kappa^3} - \frac{1}{r \kappa} \right) + \frac{j}{r^2 \kappa^2} \right) e^{j\omega_0 \tau} \\
 &= \frac{1}{4} \frac{\mu_0 m_0}{\pi} \sin(\theta) \kappa^3 \left(-\frac{1}{r \kappa} + \frac{j}{r^2 \kappa^2} + \frac{1}{r^3 \kappa^3} \right) e^{j\omega_0 \tau} \\
 &= -\frac{1}{4} j \frac{\mu_0 m_0}{\pi} \kappa^3 \sin(\theta) \left(\frac{1}{j r \kappa} + \frac{1}{j^2 r^2 \kappa^2} + \frac{1}{j^3 r^3 \kappa^3} \right) e^{j\omega_0 \tau}
 \end{aligned}$$

The field in cartesian coordinates

From the figure 2.3 we derive the following relations:

$$\begin{aligned}
 \hat{\mathbf{r}} &= \frac{\mathbf{r}}{|\mathbf{r}|} \\
 \hat{\boldsymbol{\theta}} &= \frac{(\mathbf{m} \times \mathbf{r}) \times \mathbf{r}}{|(\mathbf{m} \times \mathbf{r}) \times \mathbf{r}|}
 \end{aligned}$$

and the magnetic dipole vector is the projection on the two versors:

$$\mathbf{m} \cdot \hat{\mathbf{r}} = m_0 \cos(\theta)$$

$$\mathbf{m} \cdot \hat{\boldsymbol{\theta}} = -m_0 \sin(\theta)$$

thus equation 2.21 becomes:

$$\begin{aligned}
 \mathbf{B} &= \frac{\mu_0}{4\pi r^3} (2m_0 \cos(\theta) \hat{\mathbf{r}} + m_0 \sin(\theta) \hat{\boldsymbol{\theta}}) \\
 &= \frac{\mu_0}{4\pi r^3} (2(\mathbf{m} \cdot \hat{\mathbf{r}}) \hat{\mathbf{r}} - (\mathbf{m} \cdot \hat{\boldsymbol{\theta}}) \hat{\boldsymbol{\theta}}) \\
 &= \frac{\mu_0}{4\pi r^3} (3(\mathbf{m} \cdot \hat{\mathbf{r}}) \hat{\mathbf{r}} - (\mathbf{m} \cdot \hat{\mathbf{r}}) \hat{\mathbf{r}} - (\mathbf{m} \cdot \hat{\boldsymbol{\theta}}) \hat{\boldsymbol{\theta}}) \\
 &= \frac{\mu_0}{4\pi r^3} (3(\mathbf{m} \cdot \hat{\mathbf{r}}) \hat{\mathbf{r}} - \mathbf{m})
 \end{aligned}$$

putting the last equation in an analytical math engine, we derive this compact version, using as notation $\mathbf{r} = [x, y, z]^T$:

$$\mathbf{B} = \frac{\mu_0}{4\pi r^5} \begin{bmatrix} 2x^2 - y^2 - z^2 & 3xy & 3xz \\ 3xy & 2y^2 - x^2 - z^2 & 3yz \\ 3xz & 3yz & 2z^2 - x^2 - y^2 \end{bmatrix} \mathbf{m} \quad (2.43)$$

2.5.3 Antenna transfer function

It is easy to derive transfer function, if we consider the system as a voltage divider:

$$\begin{aligned} \frac{V_{\text{out}}}{V_{\text{ind}}} &= \frac{(R_L \parallel Cs)}{(R_L \parallel Cs) + (R_P \parallel Ls)} \\ &= \frac{\frac{1}{R_L} + Cs}{\frac{1}{R_L} + Cs + \frac{1}{R_P} + \frac{1}{Ls}} \\ &= \frac{\frac{1}{R_P} + \frac{1}{Ls}}{\frac{1}{R_L} + Cs + \frac{1}{R_P} + \frac{1}{Ls}} \\ &= \frac{1}{R_P C} \frac{s + \frac{R_P}{L}}{s^2 + \frac{1}{C R_P R_L} s + \frac{1}{LC}} \end{aligned} \quad (2.44)$$

3

Drone Avionics

Contents

3.1	Perception Action paradigm	44
3.1.1	The basic paradigm	44
3.1.2	Exploiting more complex behavior	45
<i>Expanding PA</i>	45	
<i>Subsumption and grounding</i>	45	
<i>Innate knowledge and emulation</i>	45	
<i>Bootstrapping and more</i>	45	
3.2	Building the PA map of the drone	46
3.2.1	Overview of our searching map	46
3.3	Hexa-copter model	47
3.3.1	Motion equations	47
<i>External force and torque analysis</i>	47	
<i>Inertial analysis</i>	49	
<i>Newton–Euler equations</i>	50	
3.3.2	Linearization and LQR control	51
<i>Linearization</i>	51	
<i>LQR on complete state</i>	52	
<i>Solving tracking problem</i>	52	
3.4	Obstacle avoidance	53
<i>Model of range finder</i>	54	
3.5	Altitude keeping	56
3.5.1	Kalman Filter	56
<i>Initial state probability</i>	57	
<i>Prediction phase</i>	57	
<i>Estimation state</i>	57	
<i>Complete KF algorithm</i>	58	
3.5.2	Application to altitude keeping	58
3.6	The signal detection problem	59
3.6.1	Supervised signal detection	60
3.6.2	Risk criterion	60
<i>Minimum risk criterion</i>	60	
<i>The feature space</i>	62	
3.7	Searching for the signal	63

3.8	Source searching algorithm	65
3.8.1	Exploration step	65
3.8.2	Emulation step	66
	<i>Optimization</i>	66
	<i>Estimation</i>	67

In this chapter we explore the searching algorithm applied to a dynamic simulated device really close to our drone. The simulation will use a simpler control model (LQR) and will implement the perception action paradigm for the searching part. Searching part will be performed with device implemented in previous chapter, with auxiliary range finder for obstacle avoidance and altitude keeping. All those elements build what is called avionic framework of the drone. The basic idea is to create a stacked structure that could be easily expanded in future; again, what we are discussing in an initial platform that could be improved with the use of more increasingly complex sensor-fusion, that allows to exploit the most sophisticated searching algorithm possible.

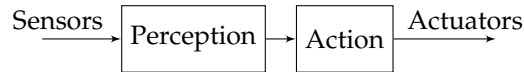
3.1 Perception Action paradigm

The perception-action (PA) paradigm has a very strict connection with the definition of our searching algorithm. Lets try to understand what is this paradigm.

3.1.1 The basic paradigm

Leaving aside the first idea of PA maps, from the 1970, if we see simply consider the blocks that form it, we understand how it is possible to build avionics on those principle. A PA map consider an agent in which external stimuli derive from a sensor network, that perform the perception section of the agent. Perception is therefore translated into a symbol that could be handled by the action section of the agent.

Figure 3.1: Classical perception-action map



Making a straight example on our device, if we consider as sensor elements our digital ARTVA, the device should represent the sensor input to the perception stage, that should analyzed to perform an action, that is the movement of the drone towards buried position.

The relationship between the agent and the environment is called *situatedness*, while the intercourse within what represents the *body* on what represents the *mind* of the agent is called *embodiment*, as explained in [4].

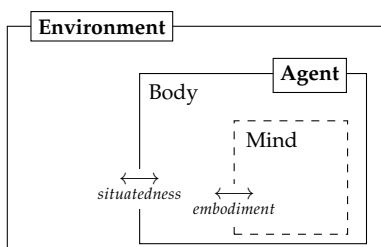


Figure 3.2: Embodiment and situatedness

3.1.2 Exploiting more complex behavior

Expanding PA

Apart the basic behavior the advantages of PA maps are related too the implementation of extremely complex actions using advances techniques such as:

- subsumption and grounding
- innate knowledge
- bootstrapping
- historical knowledge
- shared knowledge

All those element could be serially implemented, one after the other, while they run together to create a coherent attitude with respect to the problem. One of the advanced feature that we will use in this project is the subumption and the grounding of the symbols.

Subsumption and grounding

The *symbols grounding* is an implementation of the embodiment of the agent as a stacked architecture in which different layer (subsumption), that performs different operations, are piled up in such a way that higher level, of higher complexity, could transparently use lower levels (symbols grounding [9]), and incorporate them to reach their objective.

As an example, the very basic level that could be implemented is a stabilization control, that could be used to keep the plant in a controllable state. From this layer, an upper tracking layer will try to reduce the input error using the lower layer to preserve a safe stability for the system.

This techniques, introduced in [5], will be used in our avionics definition.

Innate knowledge and emulation

Evolution and generalization of the map are referred to the embodiment, with the implementation of an innate knowledge, that may be used to perform an internal emulation of the perceived environment. A typical example of this is the co-driver model implemented in [8], where emulation, defined as a mathematical model, is used to infer driver actions.

This techniques is also implemented in our avionics.

Bootstrapping and more

In this paragraph, for completeness, we could cite other techniques that generalize embodiment and situatedness. One of the most recent generalization approach is called *bootstrapping*. From [20] and [19], a cognitive system should identify and define its motion primitives.

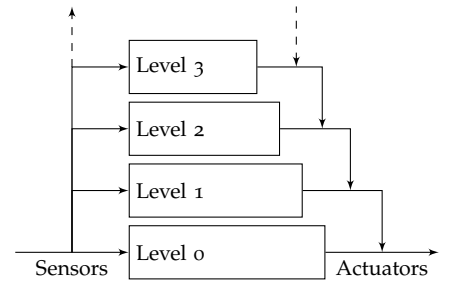


Figure 3.3: Subsumption and grounding architecture

Even if this procedure is clearly different from innate knowledge, the implementation of this technique do not exclude the implementation of some kind of innate knowledge.

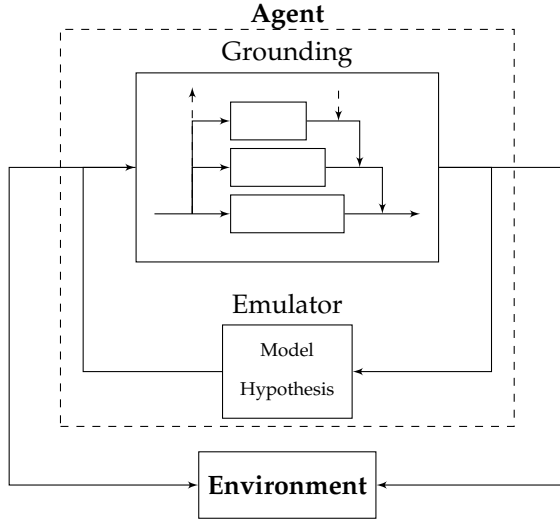


Figure 3.4: Emulation in an agent

The exploration of motion domain is performed through the use of random inputs and fuzzy logic[22] on perception:

- random exploration gives an initial model for the primitives
- repetition on the primitives allows the system to remove redundancies
- further repetition remove unused parameters
- last repetitions allows to perform an optimization and update of the model parameters

3.2 Building the PA map of the drone

3.2.1 Overview of our searching map

In figure 3.5 a comprehensive version of the map is presented. The map shows a tri-dimensional evolution in the upper side, where two different aims are achieved. On one side we have the searching for the signal, and on the other side we have the searching for the signal source. This particular design in the map was implemented to grant to the avionics the ability to perform a sort of reasoning and reach a multiple objective, as it will be explained later on.

The drone has a complex control system, already implemented in IMU shield, that takes in consideration a linearized feedback that feeds an LQR control loop [citep](#).

The system could be modified to solve a tracking problem, that will be used by the upper level. The tracking problem uses transparently the stabilization layer and it is used by the searching layer.

Upper layers, obstacle avoiding and altitude keeping, preserve drone to collide with isolated obstruction and at an altitude that is safe for rescuers.

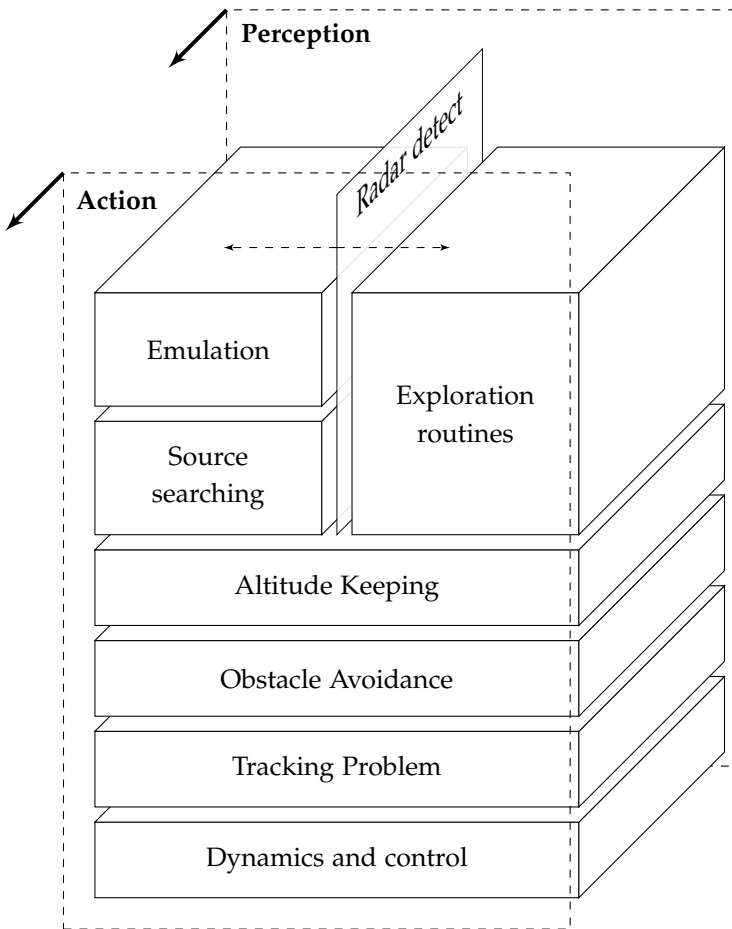


Figure 3.5: General Perception–Action map for our drone

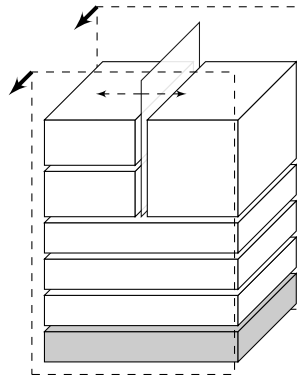
3.3 Hexa-copter model

The drone could be modeled with dynamical equations. The derivation of those equation will be performed from force analysis and control scheme is derived. A C version of the model, to be used in simulations is presented.

3.3.1 Motion equations

The system is governed by Euler–Newton equations, simplified with the imposition of the center of motion for Euler equations in center of mass of the drone. With character g we refer to global coordinate system, while with b we identify the coordinate system, that is attached to body and has origin in CoM:

$$\begin{cases} \mathbf{F}_g = m\ddot{\mathbf{x}}_g \\ \mathbf{T}_g = \dot{\mathbf{K}}_g + \dot{\mathbf{x}}_g \times \mathbf{Q}_g \end{cases} \rightarrow \begin{cases} \mathbf{F}_b = m\ddot{\mathbf{a}}_b \\ \mathbf{T}_b = \dot{\mathbf{K}}_b \end{cases} \quad (3.1)$$



External force and torque analysis

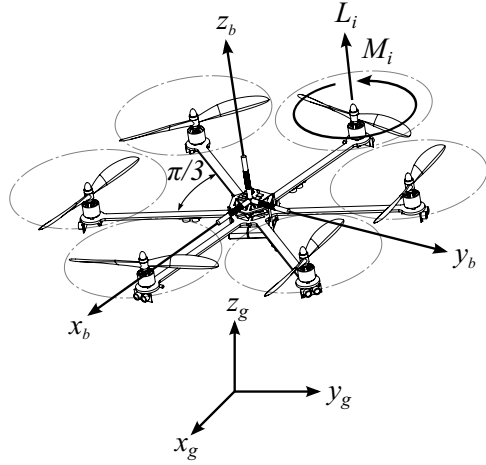


Figure 3.6: Hexa-copter kinematics

There are several force that act on the body of the drone:

$$\mathbf{F}_b = \sum_{\text{external}} F_b \quad (3.2)$$

Weight:

$$\mathbf{P}_g = \begin{bmatrix} 0 \\ 0 \\ -mg \end{bmatrix} \quad (3.3)$$

Motor thrust:

$$\mathbf{L}_b = \sum_{i=1}^6 \begin{bmatrix} 0 \\ 0 \\ -L_{b,i} \end{bmatrix} \quad (3.4)$$

Total force:

$$\mathbf{F}_b = \begin{bmatrix} \sin(\theta) \\ -\sin(\phi) \cos(\theta) \\ -\cos(\phi) \cos(\theta) \end{bmatrix} mg + \begin{bmatrix} 0 \\ 0 \\ -\sum_{i=1}^6 L_{b,i} \end{bmatrix} \quad (3.5)$$

For what concerns total external torque applied to the system:

$$\mathbf{T}_{b,0} = \sum_{\text{external}} M_b + \sum_{\text{external}} (\mathbf{p}_b - \mathbf{0}) \times \mathbf{F}_b \quad (3.6)$$

Thrust torque, with l distance between center of propeller and CoM

$$\mathbf{M}_b = \sum_{i=0}^5 \begin{bmatrix} l \cos(i\pi/3) \\ l \sin(i\pi/3) \\ 0 \end{bmatrix} \times \mathbf{L}_{b,i} \quad (3.7)$$

Drag torque, with β the proportional factor between thrust and drag torque

$$\mathbf{D}_b = \sum_{i=1}^6 \begin{bmatrix} 0 \\ 0 \\ \beta L_{b,i} \end{bmatrix} \quad (3.8)$$

In general, the total torque is:

$$\mathbf{T}_{b,0} = \begin{bmatrix} -\frac{\sqrt{3}}{2}l(L_2 + L_3 - L_5 - L_6) \\ \frac{1}{2}l(2L_1 + L_2 - L_3 - 2L_4 - L_5 + L_6) \\ \beta(L_1 - L_2 + L_3 - L_4 + L_5 - L_6) \end{bmatrix} \quad (3.9)$$

Inertial analysis

We could define speed vector in body system of coordinates:

$$\begin{bmatrix} \dot{x} \\ \dot{y} \\ \dot{z} \end{bmatrix} = \mathcal{R}(\phi, \theta, \psi) \begin{bmatrix} u \\ v \\ w \end{bmatrix} \quad (3.10)$$

. that allows us to define the accelerations vector in the form:

$$\mathbf{a}_b = \dot{\mathbf{v}}_b + \boldsymbol{\omega}_b \times \mathbf{v}_b \quad (3.11)$$

The relation that connects angular ratios in body coordinates and ground coordinates are derived from the so called *Gimbail's relations*¹:

$$\boldsymbol{\omega}_b = \mathcal{R}_x(\phi)\dot{\phi}\hat{\mathbf{e}}_x'' + \mathcal{R}_x(\phi)\mathcal{R}_y(\theta)\dot{\theta}\hat{\mathbf{e}}_y' + \mathcal{R}_x(\phi)\mathcal{R}_y(\theta)\mathcal{R}_z(\psi)\dot{\psi}\hat{\mathbf{e}}_z \quad (3.12)$$

that is simplified in the matrix form:

$$\begin{bmatrix} p \\ q \\ r \end{bmatrix} = \begin{bmatrix} 1 & 0 & -\sin(\theta) \\ 0 & \cos(\phi) & \sin(\phi)\cos(\theta) \\ 0 & -\sin(\phi) & \cos(\phi)\cos(\theta) \end{bmatrix} \begin{Bmatrix} \dot{\phi} \\ \dot{\theta} \\ \dot{\psi} \end{Bmatrix}$$

that through inversion gives:

$$\begin{Bmatrix} \dot{\phi} \\ \dot{\theta} \\ \dot{\psi} \end{Bmatrix} = \begin{bmatrix} 1 & \frac{\sin(\phi)\sin(\theta)}{\cos(\theta)} & \frac{\cos(\phi)\sin(\theta)}{\cos(\theta)} \\ 0 & \cos(\phi) & -\sin(\phi) \\ 0 & \frac{\sin(\phi)}{\cos(\theta)} & \frac{\cos(\phi)}{\cos(\theta)} \end{bmatrix} \begin{bmatrix} p \\ q \\ r \end{bmatrix} \quad (3.13)$$

The rotational matrix form body to ground is obtained through a sequence of elementary rotations: $\mathcal{R} = \mathcal{R}_z(\psi)\mathcal{R}_y(\theta)\mathcal{R}_x(\phi)$

¹Just a clarification on the notation used. Square parentheses [...] identifies vector element that belongs to the same basis, while vectorial elements in curly brackets {\cdot} do not share the same basis

For what concerns angular inertia in body reference frame:

$$\begin{aligned}\dot{\mathbf{K}}_b &= \mathbf{I}_b \dot{\boldsymbol{\omega}}_b + \boldsymbol{\omega}_b \times \mathbf{I}_b \boldsymbol{\omega}_b \\ &= \begin{bmatrix} I_x \dot{p} \\ I_y \dot{q} \\ I_z \dot{r} \end{bmatrix} + \begin{bmatrix} (I_z - I_y)qr \\ (I_x - I_z)pr \\ (I_y - I_x)pq \end{bmatrix} \quad (3.14)\end{aligned}$$

Newton–Euler equations

Defined state vectors and control vectors:

$$\begin{aligned}\mathbf{x} &= [x, y, z, u, v, w, \phi, \theta, \psi, p, q, r]^T \\ \mathbf{u} &= [L_1, L_2, L_3, L_4, L_5, L_6]^T\end{aligned}$$

we get the following Newton–Euler equations that describes dynamical behavior of the drone:

$$\left\{ \begin{array}{lcl} \dot{x} & = & \cos(\psi) \cos(\theta)u + \sin(\psi) \cos(\theta)v - \sin(\theta)w \\ \dot{y} & = & \cos(\psi)u \sin(\theta) \sin(\phi) + \sin(\psi)v \sin(\theta) \sin(\phi) + \\ & & + \cos(\psi)v \cos(\phi) + \cos(\theta) \sin(\phi)w - u \sin(\psi) \cos(\phi) \\ \dot{z} & = & \cos(\psi)u \sin(\theta) \cos(\phi) + \sin(\psi)v \sin(\theta) \cos(\phi) + \\ & & - \cos(\psi)v \sin(\phi) + \cos(\theta) \cos(\phi)w + u \sin(\psi) \sin(\phi) \\ \dot{u} & = & -q w + r v + g \sin(\theta) \\ \dot{v} & = & -r u + p w - g \sin(\phi) \cos(\theta) \\ \dot{w} & = & -p v + q u - g \cos(\theta) \cos(\phi) + \\ & & - \frac{1}{m} (L_1 + L_2 + L_3 + L_4 + L_5 + L_6) \\ \dot{\phi} & = & p + \frac{\sin(\phi) \sin(\theta)}{\cos(\theta)} q + \frac{\cos(\phi) \sin(\theta)}{\cos(\theta)} r \\ \dot{\theta} & = & \cos(\phi) q - \sin(\phi) r \\ \dot{\psi} & = & \frac{\sin(\phi)}{\cos(\theta)} q + \frac{\cos(\phi)}{\cos(\theta)} r \\ \dot{p} & = & -\frac{I_z - I_y}{I_x} q r - \frac{\sqrt{3}}{2} \frac{l}{I_x} (L_2 + L_3 - L_5 - L_6) \\ \dot{q} & = & -\frac{I_x - I_z}{I_y} p r + \frac{1}{2} \frac{l}{I_y} (2L_1 + L_2 - L_3 - 2L_4 - L_5 + L_6) \\ \dot{r} & = & -\frac{I_y - I_x}{I_z} p q + \frac{\beta}{I_z} (L_1 - L_2 + L_3 - L_4 + L_5 - L_6) \end{array} \right. \quad (3.15)$$

Sym.	Description	Value
g	Gravity	9.81 kg s^{-2}
m	Mass	2 kg
I_x	x Inertia	0.008 kg m^2
I_y	y Inertia	0.01 kg m^2
I_z	z Inertia	0.05 kg m^2
β	Drag parameter	0.2 kg m^2
l	Frame arm	0.3 m

Table 3.1: Mechanicals parameters of the simulated model

3.3.2 Linearization and LQR control

Linearization

We now linearize the system feedback to get a control that stabilizes our drone:

$$\mathbf{u}_0 : \mathbf{0} = f(\mathbf{x}_0, \mathbf{u}_0) \quad (3.16)$$

that will be solved for hovering state, that is one of the most important flight routine. In a drone, hovering is not dependent with respect to vertical orientation along $\hat{\mathbf{z}}$ axis:

$$\mathbf{x} = [x_0, y_0, z_0, 0, 0, 0, 0, 0, 0, \psi_0, 0, 0, 0]^T$$

One solution for this state is the control vector composed by thrust forces:

$$L_1 = L_2 = L_3 = L_4 = L_5 = L_6 = \frac{mg}{6}$$

and the linearized system is in the form:

$$\dot{\mathbf{x}} = \underbrace{\frac{\partial f(\mathbf{x}, \mathbf{u})}{\partial \mathbf{x}}}_{A} \Big|_{\mathbf{x}_0, \mathbf{u}_0} \mathbf{x} + \underbrace{\frac{\partial f(\mathbf{x}, \mathbf{u})}{\partial \mathbf{u}}}_{B} \Big|_{\mathbf{x}_0, \mathbf{u}_0} \mathbf{u} \quad (3.17)$$

and it is possible to obtain a representation of a linear model using a computer algebra system:

$$A = \begin{bmatrix} 0 & 0 & 0 & \cos(\psi_0) & \sin(\psi_0) & 0 & 0 & 0 & 0 & 0 & 0 & 0 \\ 0 & 0 & 0 & -\sin(\psi_0) & \cos(\psi_0) & 0 & 0 & 0 & 0 & 0 & 0 & 0 \\ 0 & 0 & 0 & 0 & 0 & 1 & 0 & 0 & 0 & 0 & 0 & 0 \\ 0 & 0 & 0 & 0 & 0 & 0 & 0 & g & 0 & 0 & 0 & 0 \\ 0 & 0 & 0 & 0 & 0 & 0 & 0 & -g & 0 & 0 & 0 & 0 \\ 0 & 0 & 0 & 0 & 0 & 0 & 0 & 0 & 0 & 0 & 0 & 0 \\ 0 & 0 & 0 & 0 & 0 & 0 & 0 & 0 & 0 & 0 & 0 & 0 \\ 0 & 0 & 0 & 0 & 0 & 0 & 0 & 0 & 0 & 0 & 1 & 0 \\ 0 & 0 & 0 & 0 & 0 & 0 & 0 & 0 & 0 & 0 & 0 & 0 \\ 0 & 0 & 0 & 0 & 0 & 0 & 0 & 0 & 0 & 0 & 0 & 1 \\ 0 & 0 & 0 & 0 & 0 & 0 & 0 & 0 & 0 & 0 & 0 & 0 \\ 0 & 0 & 0 & 0 & 0 & 0 & 0 & 0 & 0 & 0 & 0 & 0 \end{bmatrix} \quad (3.18)$$

$$B = \begin{bmatrix} 0 & 0 & 0 & 0 & 0 & 0 \\ 0 & 0 & 0 & 0 & 0 & 0 \\ 0 & 0 & 0 & 0 & 0 & 0 \\ 0 & 0 & 0 & 0 & 0 & 0 \\ 0 & 0 & 0 & 0 & 0 & 0 \\ -\frac{1}{m} & -\frac{1}{m} & -\frac{1}{m} & -\frac{1}{m} & -\frac{1}{m} & -\frac{1}{m} \\ 0 & 0 & 0 & 0 & 0 & 0 \\ 0 & 0 & 0 & 0 & 0 & 0 \\ 0 & 0 & 0 & 0 & 0 & 0 \\ 0 & -\frac{\sqrt{3}}{2} \frac{l}{I_x} & -\frac{\sqrt{3}}{2} \frac{l}{I_x} & 0 & \frac{\sqrt{3}}{2} \frac{l}{I_x} & \frac{\sqrt{3}}{2} \frac{l}{I_x} \\ \frac{l}{I_y} & \frac{1}{2} \frac{l}{I_y} & -\frac{1}{2} \frac{l}{I_y} & -\frac{l}{I_y} & -\frac{1}{2} \frac{l}{I_y} & \frac{1}{2} \frac{l}{I_y} \\ \frac{\beta}{I_z} & -\frac{\beta}{I_z} & \frac{\beta}{I_z} & -\frac{\beta}{I_z} & \frac{\beta}{I_z} & -\frac{\beta}{I_z} \end{bmatrix} \quad (3.19)$$

LQR on complete state

From our linear system:

$$\dot{\mathbf{x}} = A\mathbf{x} + B\mathbf{u} \quad (3.20)$$

given the quadratic control cost function, with infinite horizon:

$$J = \int_0^{\infty} \mathbf{x}^T Q \mathbf{x} + \mathbf{u}^T R \mathbf{u} dt$$

with Q and R positive defined. The optimum control that minimize this functional is:

$$\mathbf{u}^* = -R^{-1}B^T P \mathbf{x} \quad (3.21)$$

where P is the solution of *Riccati's equation*:

$$A^T P + PA - PBR^{-1}B^T P + Q = 0$$

the solution of this equation is obtain through numerical tools such as Matlab's `lqr` algorithm. Unfortunately it is impossible to derive analytical solution, given a wise chose of Q and R matrix. Usually, and also in this case, it is a good idea to follow the Bryson estimation (diagonal matrix, with higher weight to Q matrix, or *cheap control*):

$$Q = \text{eye}(q_i : i = 1..12)$$

$$R = \rho \mathbb{I}_{6 \times 6}$$

whit the additional constraint to keep observability and controllability on couples:

$$\begin{aligned} \mathcal{O}(A, \sqrt{Q}) &= \text{rank} \left(\sqrt{Q}^T A^T \sqrt{Q}^T \dots (A^T)^{\dim(\mathbf{x})-1} \sqrt{Q}^T \right) = 12 \\ \mathcal{C}(A, B) &= \text{rank} \left(B A B \dots (A)^{\dim(\mathbf{x})-1} B \right) = 6 \end{aligned}$$

Solving tracking problem

It is really simple to solve a tracking problem starting from an LQR, that tries always to reach a zero. Simply insert an offset in position, and the system will try to reduce the error until it reach zero. Here we have a figure that explains the complete control, and some simulation test for random initial conditions that tries to reach a specific position in space.

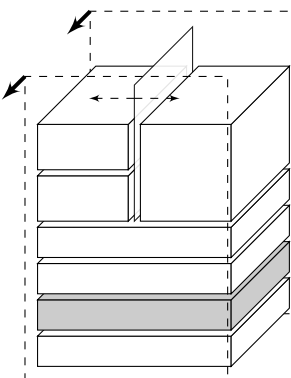
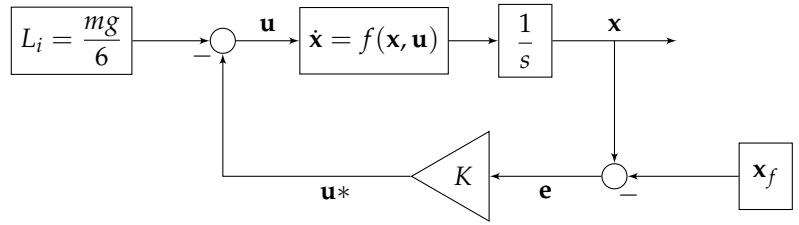


Figure 3.7: Control block scheme



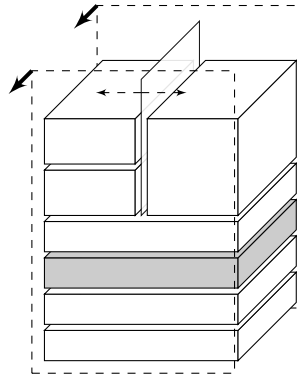
3.4 Obstacle avoidance

An avalanche has an huge amount of kinetic energy, enough to destroy most of the artificial building and move objects with a big cross-section that are on its traveling path. Thus, the objects that avalanche drone has to avoid are mainly pillars, trees or mounds of snow.

Taken into account this consideration about the surroundings in which the drone will try to find a buried person, it is useless to define an internal map of obstacle and elaborate the optimal trajectory to an ending point because, in fact, for the most of the time the drone will explore without having such a knowledge of the ending point.

This simplification gather different advantage to the final algorithm:

- we do not need the extremely high computational power needed to maintain such environment projection into agent mind space
- the obstacle avoidance imposes minor constraints on the upper layer of the searching algorithm, with respect to convoluted algorithm
- the simplification brings to a more reliable routine, because of its deterministic nature, with respect to a Bayesian based map
- this algorithm fits technical specification imposed by used hardware



while the main drawbacks are

- we are searching using an optimized domain
- it is based on a simplification, and real life is always harder than what we aspect

Diving into deep, the definition is based upon the presence of one range finder for each arm of the drone. As range finder it is possible to use ultrasonic range finders, that are device that do not have problems on lens like laser ones. An ultrasonic range finder has a characteristic lobe, similar to an antenna directivity lobe, with a peak at almost 6m.

The algorithm tries to identify a run away speed, given the distance

from the obstacle received from each sensor ($d_i : i = 1..6$):

$$\mathbf{v} = \mathcal{R}(\phi, \theta, \psi) \sum_{i=1}^6 v(d_i) \begin{bmatrix} \cos((i-1)\frac{\pi}{3}) \\ -\sin((i-1)\frac{\pi}{3}) \\ 0 \end{bmatrix} \quad (3.22)$$

where $v(d_i)$ is a function that defines the velocity magnitude on the direction of the range finder. The first magnitude used was:

$$v(d_i) = -\frac{1}{d_i} \quad (3.23)$$

that has some discontinuity problems, so the next function implemented is a sigmoid function:

$$v(d_i) = p_3 \left(\frac{1}{1 + e^{4(\frac{p_1}{2} - d_i) \frac{p_2}{p_3}}} - 1 \right) \quad (3.24)$$

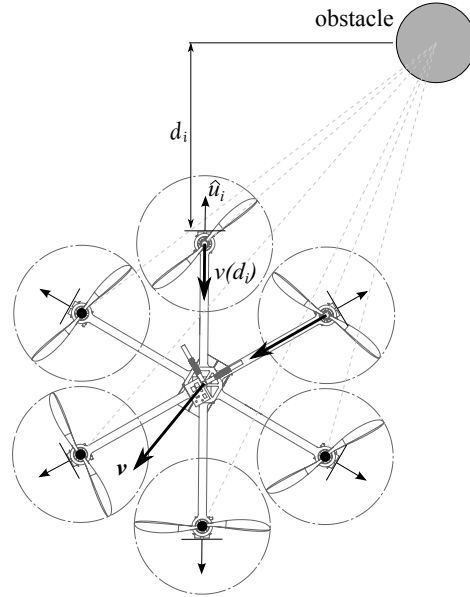
from which we obtain a continuous function were the parameters:

- p_1 : it is the maximum range, at which considered velocity is zero
- p_2 : defines the slope of the curve at $d_i = p_1/2$
- p_3 : defines the maximum velocity, or the value of the curve for $d_i = 0$

In figure 3.9 an example of how the algorithm works is shown. Obviously, signal coming from the algorithm get some sort of filtration to eliminate various source of error.

Figure 3.8: Velocity profile

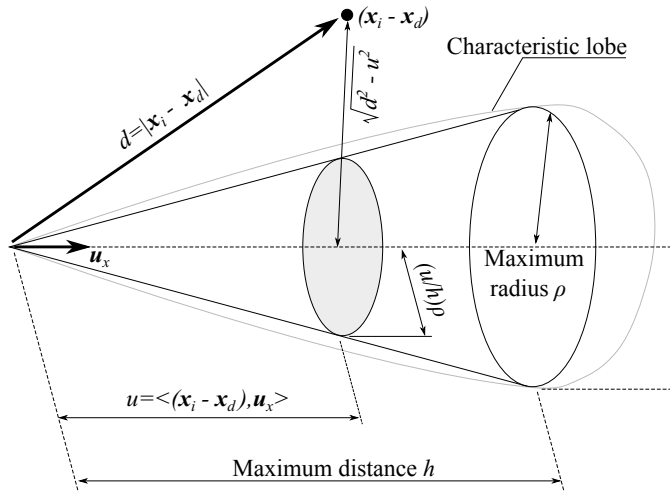
Figure 3.9: Example of obstacle avoid algorithm behavior



Model of range finder

From the simulation point of view the effects of an obstacle are obtained through a model of the characteristic lobe of each range

Figure 3.10: Range finder algorithm



finder. The obstacles are implemented as sets of points, paradigm that brings a little advantage of inserting some noise due to the discontinuities between points, similar to real range finder noise, due to analog to digital conversion.

$$\Psi = [\mathbf{x}_i : i = 1..M] \quad (3.25)$$

For our system we suppose to know exactly the position \mathbf{x}_d and orientation $\mathcal{R}(\phi, \theta, \psi)$ of the drone². We define observation versors as follows:

$$\{\hat{\mathbf{u}}_i : i = 1..6\} \rightarrow \left\{ \begin{bmatrix} \cos((i-1)\frac{\pi}{3}) \\ -\sin((i-1)\frac{\pi}{3}) \\ 0 \end{bmatrix} : i = 1..6 \right\} \quad (3.26)$$

The characteristic of the range finder is described with the use of a cone. Distance is evaluated using time of flight of an ultrasonic signal emitted by the oscillator. Mathematically it is possible to define the lobe with a cone in the space, that has axis parallel to the versors defined in 3.26, and vertex coincident with receiving system. The solid that approximates the characteristic lobe is defined by:

$$x = \frac{u}{h}\rho \cos(\theta)y = \frac{u}{h}\rho \sin(\theta)z = u \quad (3.27)$$

so characteristic lobe is defined by the parameter:

- h : receiver maximum distance
- ρ : receiver maximum lobe dimension

Given a point $\mathbf{x}_i \in \Psi$, if it is inside the cone, the projection of the distance $\mathbf{x}_d - \mathbf{x}_i$ on the axis of the cone is the identified distance.

The algorithm describes how each sensor returns the minimum identified distance that is inside its cone. The distances are used to build the velocity vector that avoid the obstacle.

² For the obstacle avoidance algorithm only attitude must be known, to project the velocity in ground reference frame

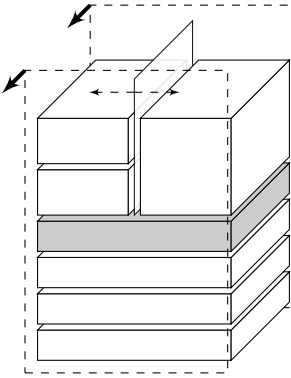
Algorithm 1: Range finder points

Data: h, ρ

```

1 foreach Obstacle as  $\Psi$  do
    /* Exec for each point of an obstacle */
    2 for  $i = 1$  to  $M$  do
        3      $\mathbf{d}_i^\Psi \leftarrow \mathcal{R}^T(\phi, \theta, \psi) (\mathbf{x}_{i, \text{ground}} - \mathbf{x}_d);$ 
        4 for  $j = 0$  to  $5$  do
            5      $D_{i,j}^\Psi \leftarrow \mathbf{d}_i^\Psi \cdot \hat{\mathbf{u}}(j\pi/3);$ 
            /* Check if the point is in cone, else distance is  $\infty$  */
            6 if  $(0 \leq D_{i,j}^\Psi \leq h)$  then
                7 if  $(\mathbf{d}_i^\Psi \cdot \mathbf{d}_i^\Psi - D_{i,j}^\Psi \geq (\frac{\rho}{h} D_{i,j}^\Psi)^2)$  then
                    8      $D_{i,j}^\Psi \leftarrow \infty;$ 
            9 else
                10      $D_{i,j}^\Psi \leftarrow \infty;$ 
        11     /* Search minimum distance for each sensor */
        12 r  $\leftarrow [r_j = \infty : j = 0$  to  $5];$ 
        13 for  $j = 0$  to  $5$  do
            14 foreach Obstacle as  $\Psi$  do
            15 for  $i = 1$  to  $M$  do
            16 if  $r_j \geq D_{i,j}^\Psi$  then
                17      $r_j \leftarrow D_{i,j}^\Psi;$ 
17 return r

```



3.5 Altitude keeping

The last basic block that should be implemented is the altitude keeping, to maintain the distance of the drone to the soil high enough to avoid contact with rescuer and low enough to get a good signal strength. The sensors used are, again, ultrasonic range finder. With respect to the obstacle avoidance, that acts as a control on the lateral dynamic of the drone, that is quite slow, altitude keeping works on vertical dynamic that is really fast, and need a more reliable implementation, and require a statistical system to determine the distance even with a high irregular terrain.

This part was actually not implemented because of the need of more test about response of ultrasonic waves upon snow surface, to better understand the effects of density on perceived distance.

3.5.1 Kalman Filter

We assume that the dimension could be described with the use of normal distribution:

$$p(\mathbf{x}) \det((2\pi)^n \Sigma_0)^{-1/2} e^{-\frac{1}{2}(\mathbf{x}-\mu)^T \Sigma^{-1} (\mathbf{x}-\mu)} \quad (3.28)$$

with μ the mean value for the distribution and Σ covariance matrix of the distribution.

The Kalman filter include the knowledge of the covariance matrix into the state estimation procedure, and it is possible to proof that the final estimation will maintain a normal distribution if:

- distribution of initial state is normal
- the state distribution is a linear function of the previous state and a white Gaussian noise
- the measurement distribution is a linear function of the state and a white Gaussian noise

Initial state probability

We make the really strong hypothesis to have an initial distribution in the normal form:

$$p(\mathbf{x}_0) \det((2\pi)^n \Sigma_0)^{-1/2} e^{-\frac{1}{2}(\mathbf{x}_0 - \mu_0)^T \Sigma_0^{-1} (\mathbf{x}_0 - \mu_0)} \quad (3.29)$$

Prediction phase

The distribution of the state derives from the distribution of the previous state, using the linear relation:

$$\mathbf{x}_t = A_t \mathbf{x}_{t-1} + B_t \mathbf{u}_t + \mathbf{w}_t \quad (3.30)$$

where \mathbf{w}_t is a realization of a distribution $\mathcal{N}(\mathbf{0}, R_t)$ in which R_t is the matrix that describes the covariance of the noise on the state.

The distribution is normal due to the relations:

$$\begin{aligned} \bar{\mu}_t &= A_t \mu_{t-1} + B_t \mathbf{u}_t \\ \bar{\Sigma}_t &= A_t \Sigma_{t-1} A_t^T + R_t \\ p(\mathbf{x}_t | \mathbf{x}_{t-1}, \mathbf{u}_t) &= \det((2\pi)^n R_t)^{-\frac{1}{2}} e^{(-\frac{1}{2}(\mathbf{x}_t - \bar{\mu}_t)^T R_t^{-1} (\mathbf{x}_t - \bar{\mu}_t))} \end{aligned}$$

If the system has a non-linear function that describes the dynamic, it could be approximated with a first-order Taylor expansion:

$$\mathbf{x}_t = g(\mathbf{x}_{t-1}, \mathbf{u}_t) + \mathbf{w}_t \quad (3.31)$$

$$\begin{aligned} \text{Taylor}_1(g(\mathbf{x}_{t-1}, \mathbf{u}_t)) \Big|_{\bar{\mu}_{t-1}, \bar{\mathbf{u}}_t} &= g(\bar{\mu}_{t-1}, \bar{\mathbf{u}}_t) + \\ &\quad \nabla_{\mathbf{x}} g(\mathbf{x}_{t-1}, \mathbf{u}_t) \Big|_{\bar{\mu}_{t-1}, \bar{\mathbf{u}}_t} (\mathbf{x}_{t-1} - \bar{\mu}_{t-1}) \\ &= g(\bar{\mu}_{t-1}, \bar{\mathbf{u}}_t) + A_t (\mathbf{x}_{t-1} - \bar{\mu}_{t-1}) \end{aligned}$$

Estimation state

The measurement distribution derives directly from the measurement model:

$$\mathbf{z}_t = C_t \mathbf{x}_t + \mathbf{v}_t \quad (3.32)$$

where \mathbf{v}_t is a realization of a distribution $\mathcal{N}(\mathbf{0}, Q_t)$ in which Q_t is the matrix that describes the covariance of the noise on the measurement.

The distribution maintains its normal behavior due to the relation:

$$p(\mathbf{z}_t | \mathbf{x}_t) = \det((2\pi)^n Q_t)^{-\frac{1}{2}} e^{(-\frac{1}{2}(\mathbf{z}_t - C_t \mathbf{x}_t)^T Q_t^{-1} (\mathbf{z}_t - C_t \mathbf{x}_t))}$$

If the measurement is modeled with the use of a non-linear function it is possible to use a Taylor expansion to approximate locally the measurement function:

$$\mathbf{z}_t = h(\mathbf{x}_t) + \mathbf{v}_t \quad (3.33)$$

$$\begin{aligned} \text{Taylor}_1(h(\mathbf{x}_t)) \Big|_{\bar{\mu}_t} &= h(\bar{\mu}_t) + \nabla_{\mathbf{x}} h(\mathbf{x}_t) \Big|_{\bar{\mu}_{t-1}} (\mathbf{x}_t - \bar{\mu}_t) \\ &= h(\bar{\mu}_t) + C_t (\mathbf{x}_t - \bar{\mu}_t) \end{aligned}$$

Complete KF algorithm

Now we are ready to define a complete Kalman Filter. The blue lines represent the step that should be performed in the case of non-linear models. Must be noticed, that in case of such non-linearities, it is impossible to demonstrate the fact that normal posterior distribution are maintained.

Algorithm 2: (Extended) Kalman Filter

```

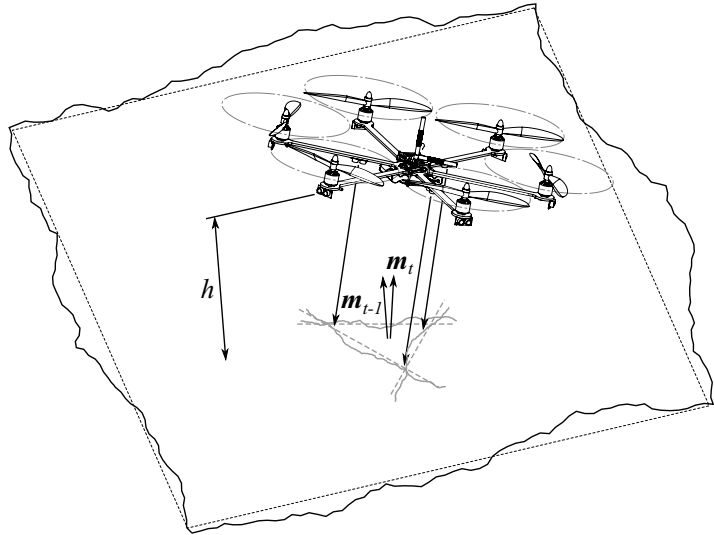
Data:  $\boldsymbol{\mu}_{t-1}, \Sigma_{t-1}, \mathbf{u}_t, \mathbf{z}_t$ 
/* Prediction phase */

1 if Model is linear then
2    $\bar{\boldsymbol{\mu}}_t = A_t \boldsymbol{\mu}_{t-1} + B_t \mathbf{u}_t$  ;
3    $\bar{\mathbf{z}}_t = C_t \bar{\boldsymbol{\mu}}_t$  ;
4 else
5    $\bar{\boldsymbol{\mu}}_t = g(\boldsymbol{\mu}_{t-1}, \mathbf{u}_t)$  ;
6    $A_t = \nabla_{\mathbf{x}} g(\mathbf{x}_{t-1}, \mathbf{u}_t) \Big|_{\bar{\boldsymbol{\mu}}_{t-1}, \mathbf{u}_t}$  ;
7    $B_t = \nabla_{\mathbf{x}} h(\mathbf{x}_{t-1}) \Big|_{\bar{\boldsymbol{\mu}}_{t-1}, \mathbf{u}_t}$  ;
8    $\bar{\mathbf{z}}_t = h(\bar{\boldsymbol{\mu}}_t)$  ;
9    $\bar{\Sigma}_t = A_t \bar{\Sigma}_{t-1} A_t^T + R_t$  ;
/* Evaluation of Kalman Gain */
10   $\mathcal{K}_t = \bar{\Sigma}_t C_t^T (C_t \bar{\Sigma}_t C_t^T + Q_t)^{-1}$  ;
/* Estimation phase */
11   $\boldsymbol{\mu}_t = \bar{\boldsymbol{\mu}}_t + \mathcal{K}_t (\mathbf{z}_t - \bar{\mathbf{z}}_t)$  ;
12   $\Sigma_t = (\mathbb{I} - \mathcal{K}_t C_t) \bar{\Sigma}_t$  ;
13 return  $\boldsymbol{\mu}_t, \Sigma_t$ 

```

3.5.2 Application to altitude keeping

Figure 3.11: Altitude keeping problem



We can model the problem taking into account attitude dynamic and vertical dynamic of the VTOL, from which we know also the rotation matrix of the drone. The plane of the avalanche could be approximated through the orthogonal versor $\hat{\mathbf{m}}$, projected in the drone reference frame. The problem, inserting $\hat{\mathbf{m}}$ into the state vector, becomes equivalent to a *SLAM*³ problem.

³ SLAM: Simultaneous Localization And Mapping

The state is:

$$\mathbf{x} = \begin{bmatrix} \mathbf{x} \\ \hat{\mathbf{m}}_b \end{bmatrix} \quad (3.34)$$

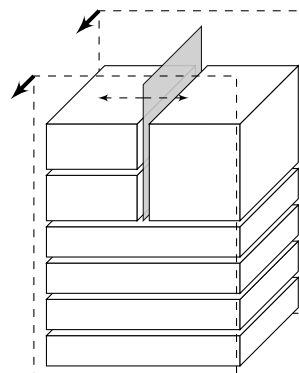
and the covariance matrix of the state derives from covariance of the position system at which must be added a covariance matrix on the knowledge of $\hat{\mathbf{m}}_b = \mathcal{R}(\phi, \theta, \psi)^T \hat{\mathbf{m}}$. We could use three range finder directed to the ground, under the drone, that allow us to define three points on the surface. A model for the measurement function uses some simple algebraic definitions: given three points that belong to the plane, $\{A, B, C\}$, the normal is:

$$\hat{\mathbf{m}} = \frac{(A - B) \times (B - C)}{|(A - B) \times (B - C)|} \quad (3.35)$$

Once normal is known, it could be used to implement a tracking control that maintains a certain distance on the normal vector. As already said, the performance of this algorithm depends directly from the estimation of the covariance matrix for measurement, and upon the sonar response due to variation of snow on the field.

3.6 The signal detection problem

We have two searching status for our agent. In one searching status, the VTOL tries to identify a signal, while in the second stage, once we have identified the presence of a signal, the drone has to find the transmission source point. The passage from a searching strategy to another is the *supervised signal detection*.



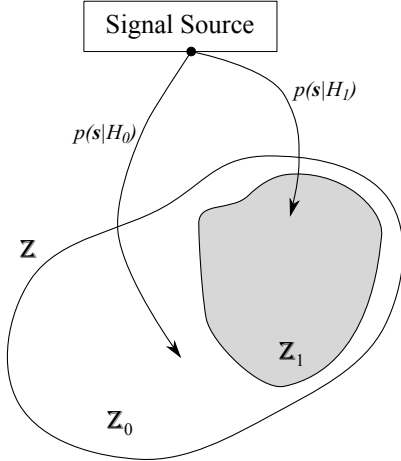


Figure 3.12: Decision spaces

3.6.1 Supervised signal detection

What we are trying to define is a strategy that is able to detect a target signal from a background noise. This is not new to signal theory, if we look at radar research work.

The detection theory is seen as a binary classification problem based upon two hypothesis:

- hypothesis 0: absence of signal
- hypothesis 1: presence of signal

The choice is made upon a signal $\mathbf{s} = [s_1, \dots, s_n]$ in which a certain number of feature identifies its belonging to a decision field or observation space $Z \in \mathbb{R}^n$. The observation space is defined by the union of two decision regions:

$$Z \equiv Z_0 \cup Z_1$$

Each decision space has a conditional PDF, that is assumed to be known:

$$Z_0 \mapsto p(\mathbf{s}|H_0)$$

$$Z_1 \mapsto p(\mathbf{s}|H_1)$$

3.6.2 Risk criterion

The classification is based upon criteria, such as:

- Minimum Risk Criterion
- Minimax Criterion
- Neyman–Pearson Criterion

That represents the classification strategies.

	Decide absent D_0	Decide present D_1
Signal absent H_0	Correct rejection: $c_{0,0}$	False alarm: $c_{1,0}$
Signal present H_1	Miss: $c_{0,1}$	Hit: $c_{1,1}$

Table 3.3: Costs matrix

Minimum risk criterion

This criterion is based upon the assumptions that posteriors probability $P(H_0|\mathbf{s})$ and $P(H_1|\mathbf{s})$ are known, and also the cost matrix is known, where the matrix is defined in table 3.3.

In practice we have: $c_{0,1} > c_{1,1}$ and $c_{1,0} > c_{0,0}$.

The main objective is to minimize the average cost incurred by erroneous decision [citep libro pattrec](#). This is done through a minimization of a risk function defined over observation space. This optimization allows us to define the decision regions Z_0 and Z_1 which are optimal in terminal of overall risk. We define the risk:

$$R = c_{0,0}P(D_0, H_0) + c_{1,0}P(D_1, H_0) + c_{0,1}P(D_0, H_1) + c_{1,1}P(D_1, H_1) \quad (3.36)$$

using the axiom of probability on $P(D_i, H_j)$, we get in general:

$$P(D_i, H_j) = P(D_i|H_j)P(H_j) \quad (i, j) \in (0..1, 0..1) \quad (3.37)$$

and also:

$$P(D_i|H_j) = \int_{Z_i} P(\mathbf{s}|H_j)d\mathbf{s} \quad (3.38)$$

The evaluation, for each conditional probability is:

$$P(D_0|H_0) = \int_{Z_0} p(\mathbf{s}|H_0)d\mathbf{s} = 1 - P_F$$

$$P(D_0|H_1) = \int_{Z_0} p(\mathbf{s}|H_1)d\mathbf{s} = P_M$$

$$P(D_1|H_0) = \int_{Z_1} p(\mathbf{s}|H_0)d\mathbf{s} = P_F$$

$$P(D_1|H_1) = \int_{Z_1} p(\mathbf{s}|H_1)d\mathbf{s} = 1 - P_M$$

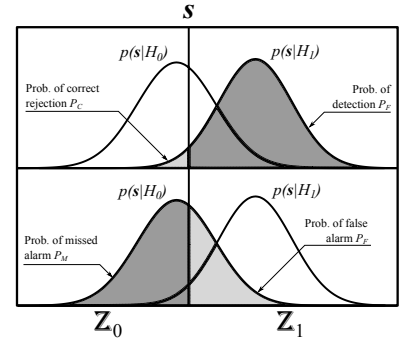


Figure 3.13: Probability versus decision space

where:

- P_C : represents probability of correct rejection
- P_F : represents probability of false alarm
- P_M : represents probability of missed alarm
- P_D : represents probability of detection

and, looking at figure ??, stands the relation:

$$P_D + P_M = 1$$

$$P_C + P_F = 1$$

Finally, we get the definition of risk:

$$\begin{aligned} R &= c_{0,0}(1 - P_F)P(H_0) + c_{0,1}P_M P(H_1) + \\ &\quad + c_{1,0}P_F P(H_0) + c_{1,1}(1 - P_M)P(H_1) \\ &= P(H_0)(c_{0,0} + P_F(c_{1,0} - c_{0,0})) + P(H_1)(c_{1,1} + P_M(c_{0,1} - c_{1,1})) \end{aligned} \quad (3.39)$$

applying some substitutions:

$$\begin{aligned} P_M &= \int_{Z_0} p(\mathbf{s}|H_1)d\mathbf{s} \\ P_F &= \int_{Z_1} p(\mathbf{s}|H_0)d\mathbf{s} = \\ &= 1 - \int_{Z_0} p(\mathbf{s}|H_0)d\mathbf{s} \\ 1 &= \int_{Z_0} p(\mathbf{s}|H_j)d\mathbf{s} + \int_{Z_1} p(\mathbf{s}|H_j)d\mathbf{s} \end{aligned}$$

and the risk equation:

$$\begin{aligned}
R &= P(H_0)(c_{0,0} + P_F(c_{1,0} - c_{0,0})) + P(H_1)(c_{1,1} + P_M(c_{0,1} - c_{1,1})) = \\
&= P(H_0) \left(c_{0,0} + \left(1 - \int_{\mathbb{Z}_0} p(\mathbf{s}|H_0) d\mathbf{s} \right) (c_{1,0} - c_{0,0}) \right) + \\
&\quad + P(H_1) \left(c_{1,1} + \left(\int_{\mathbb{Z}_0} p(\mathbf{s}|H_1) d\mathbf{s} \right) (c_{0,1} - c_{1,1}) \right) = \\
&= P(H_0)c_{1,0} + P(H_1)c_{1,1} + \\
&\quad + \int_{\mathbb{Z}_0} P(H_1)(c_{0,1} - c_{1,1}) p(\mathbf{s}|H_1) - P(H_0)(c_{1,0} - c_{0,0}) p(\mathbf{s}|H_0) d\mathbf{s}
\end{aligned} \tag{3.40}$$

The first part is constant, to minimize the risk we have to work on the argument of the integral, that depends upon \mathbb{Z}_0 . Because:

$$P(H_1)(c_{0,1} - c_{1,1}) p(\mathbf{s}|H_1) \geq 0$$

$$P(H_0)(c_{1,0} - c_{0,0}) p(\mathbf{s}|H_0) \geq 0$$

the risk is minimized when:

$$P(H_1)(c_{0,1} - c_{1,1}) p(\mathbf{s}|H_1) < P(H_0)(c_{1,0} - c_{0,0}) p(\mathbf{s}|H_0) \tag{3.41}$$

and rearranged as follow

$$\frac{p(\mathbf{s}|H_1)}{\underbrace{p(\mathbf{s}|H_0)}_{\Lambda(\mathbf{s})}} < \underbrace{\frac{P(H_0)(c_{1,0} - c_{0,0})}{P(H_1)(c_{0,1} - c_{1,1})}}_{\eta} \tag{3.42}$$

that allow us to define the algorithm 3. Must be noticed:

- because of the binary nature, the decision rule obtained with the minimization on a single decision, grant the minimization of the risk also on the other decision; thus we could say that the local decision rule minimizes the overall risk
- the likelihood ratio and threshold define decision regions as follows:

$$\mathbb{Z}_0 = \{\mathbf{s} \in \mathbb{Z} : \Lambda(\mathbf{s}) < \eta\}$$

$$\mathbb{Z}_1 = \{\mathbf{s} \in \mathbb{Z} : \Lambda(\mathbf{s}) > \eta\}$$

and a sample such that $\Lambda(\mathbf{s}) = \eta$ could be assigned arbitrarily to one of the decision region

- the distributions $p(\mathbf{s}|H_0)$ and $p(\mathbf{s}|H_1)$ should be derived experimentally, something that is not to difficult because of characteristics of our signal

The feature space

The feature space that could be used are the three signal received from the three orthogonal antennas, plus the position. Te insertion of the position in the feature space is not important for the actual

Algorithm 3: Minimum risk criterion

Data: $p(\mathbf{s}|H_1)$, $p(\mathbf{s}|H_0)$, $c_{0,0}$, $c_{1,0}$, $c_{0,1}$, $c_{1,1}$

```

/* Define the likelihood ratio */
1  $\Lambda(\mathbf{s}) \leftarrow \frac{p(\mathbf{s}|H_1)}{p(\mathbf{s}|H_0)}$ ; /*

/* Define the threshold */
2  $\eta \leftarrow \frac{P(H_0)(c_{1,0} - c_{0,0})}{P(H_1)(c_{0,1} - c_{1,1})}$ ; /*

/* Binary classification */
3 forall the  $\mathbf{s}_{in}$  do
4   if  $\Lambda(\mathbf{s}_{in}) \leq \eta$  then
5     return  $\mathbf{s} \in H_0$ 
6   else
7     return  $\mathbf{s} \in H_1$ 

```

implementation, but could be useful in future, if some computer vision algorithm will be implemented. Algorithms that are able to represent symbolically the dimensions of the avalanche front, in conjunction with slope of the avalanche obtained by the altitude keeping routine, may allow us to define a probability distribution of the possible buried victims, distribution that could be inserted as a priori knowledge in radar detection and searching algorithm.

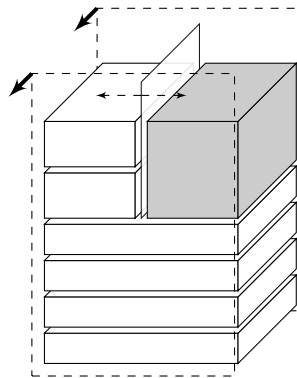
3.7 Searching for the signal

In this section we derive a very simple method to cover the avalanche front to search for a signal beacon. The algorithm presented is incredibly simple and derives from what is actually done by a rescuer on the avalanche front. We try to cover the area of the avalanche with straight equi-spaced lines generated from a series of points.

When turned on, the drone require insertion of two GPS coordinates, or and a direction from the rescuer. Those two coordinates represent starting point and ending point for the first level of search. Those two points defines a rectangle, the direction represent the orientation of the rectangle. Those data could be inserted from a media device such as tablet or smartphone.

Once the search area is defined, it is divided into a regular grid, identified by points in the center of each square of the grid. Due to the fact that such input derives from an external device that has computational power, we could use this external device to perform such calculation.

Once the points array is defined, drone simply uses the lower levels of the map to reach each point in sequence. In some cases may be impossible to reach the specific point, due to causes like obstacle or uncertainty due to the motion. To avoid this problem, for each point, is associated a confidence distance, that defines a sphere in which the drone should fly before going to the next point. When last point



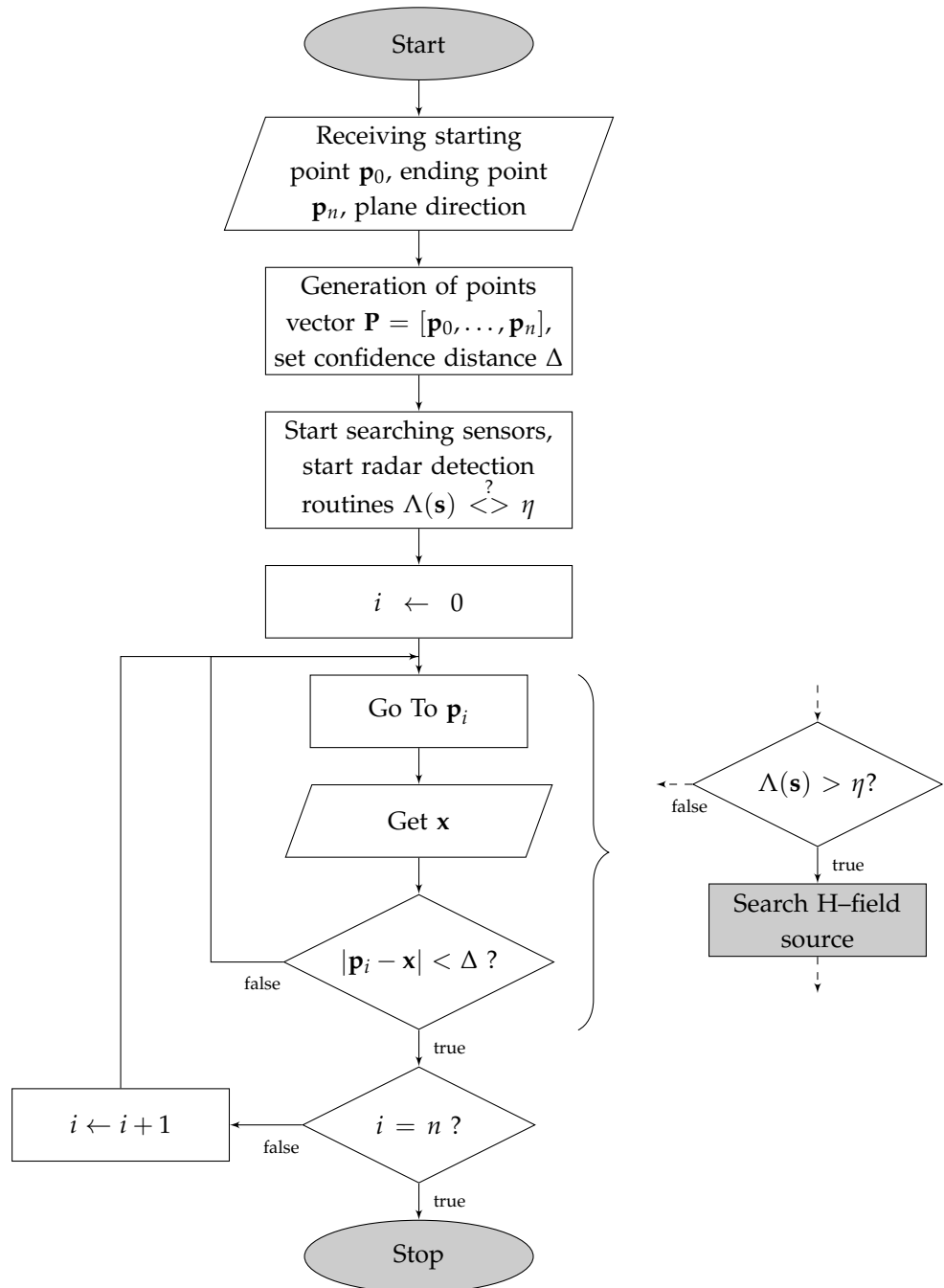


Figure 3.14: Exploration algorithm

is reached mission is over. A flowchart of algorithm is presented in figure 3.14.

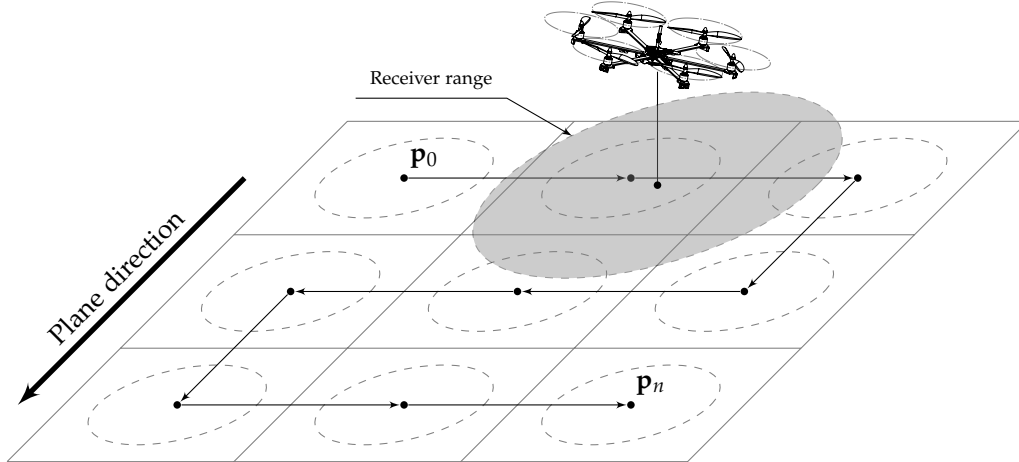


Figure 3.15: Subdivision of the searching plane

3.8 Source searching algorithm

Some new papers in searching suggested the use of a modified version of the *SLAM* problem to identify position of the source and direction of the dipole. Even if some promising results are exposed in cited papers [16, 17], we were not able to reproduce such results with our system in simulations; because of that, we decided to drop this approach to use one that fit better the perception–action paradigm.

The proposed algorithm uses a two component algorithm.

3.8.1 Exploration step

The first step is simply an adaptive filter, stolen from the evaluation of Round-Trip-Time in TCP networking, that tries to identify a direction in which the signal is maximized, given an adapted previous knowledge. The algorithm takes into consideration the presence of fluctuations due to noise and interference and changes orientation only when the change in signal is obvious. Scaling parameter regulate the velocity that will move the drone.

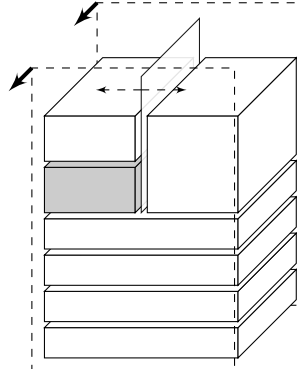
An adaptive filter for a variable x is defined as:

$$x_k = \alpha x_{k-1} + (1 - \alpha) \hat{x}_k \quad 0 \leq \alpha \leq 1$$

The first part is a mean sampler, that helps us to partially eliminate the white Gaussian noise:

$$\hat{\mathbf{H}}_g = \frac{1}{N} \mathcal{R}(\phi, \theta, \psi) \sum_{i=0}^N \mathbf{H}_{b,i} \quad (3.43)$$

Starting from the vector of received signal \mathbf{H} , the value measured is a vector in hexa-copter body reference frame, and should be reported in ground reference frame, using the state of the drone. From the



projection of the H-field some information are extracted, like **intensity** and **direction on $(\hat{x} \times \hat{y})$ plane**:

$$\begin{aligned}\cos(\alpha) &= \cos(\arctan_2(H_y, H_x)) \\ \sin(\alpha) &= \sin(\arctan_2(H_y, H_x)) \\ |\mathbf{H}| &= \sqrt{H_x^2 + H_y^2 + H_z^2}\end{aligned}\quad (3.44)$$

The next step is a filtering to eliminates some of the residual noise, with a second order filter. We exploit the discontinuity problem of the $\arctan_2(\cdot)$ function using trigonometric functions. From the input values:

- the value of the measured field is used to steer the system in direction of the source, to avoid symmetric problem of the received field
- the adapted H-field measurement defines the speed, through a function $v(\cdot)$
- the direction of speed is defined using adapted angle

The effect of this routine is only to explore the environment in a direction the maximizes the received signal.

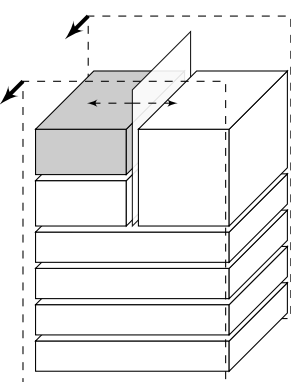
Algorithm 4: Searching and explore

```

Data:  $|\mathbf{H}|_{k-1}, \psi_{k-1}, \mathbf{v}_{k-1}, w_1, w_2, \Delta, \delta$ 
/* Steer in direction of greater intensity */

1 if  $\left( \frac{|\mathbf{H}|_k}{|\mathbf{H}|_{k-1}} - 1 \right) \leq \Delta$  then
2    $\psi_k = (1 - w_1)\psi_{k-1} + w_1\delta;$ 
3 else if  $\left( \frac{|\mathbf{H}|_k}{|\mathbf{H}|_{k-1}} - 1 \right) \geq \Delta$  then
4    $\psi_k = (1 - w_1)\psi_{k-1} - w_1\delta;$ 
/* Set speed magnitude */
5  $|\mathbf{v}_k| = (1 - w_2)|\mathbf{v}_{k-1}| + w_2v(|\mathbf{H}_k|);$ 
/* Steer in direction of flux lines */
6  $\cos(\psi)_k = (1 - w_1)\cos(\theta) + w_1\cos(\psi)_{k-1};$ 
7  $\sin(\psi)_k = (1 - w_1)\sin(\theta) + w_1\sin(\psi)_{k-1};$ 
/* Defines speed */
8  $\mathbf{v}_k = \begin{bmatrix} |\mathbf{v}_k| \cos(\psi)_k \\ |\mathbf{v}_k| \sin(\psi)_k \\ 0 \end{bmatrix};$ 
9 return  $\mathbf{v}_k$ 

```



3.8.2 Emulation step

Optimization

In parallel with the previous searching method, an emulation of the real field is implemented. The emulation tries to understand the position of the source as a solution of an optimization problem, using

previous solution as a guess that is adapted through time. The optimization problem is:

$$\begin{aligned} & \arg \min_{\mathbf{p}_T} \quad \delta \\ & \text{subject to} \quad \left\{ \begin{array}{l} \delta = (\mathbf{H}(\mathbf{x}, \mathbf{p}_T, \mathbf{m}) - \hat{\mathbf{H}})^2 \\ (\mathbf{x} - \mathbf{p}_T)^2 \leq r_{\max} \end{array} \right. \end{aligned} \quad (3.45)$$

The optimization problem is solved numerically, guessing as initial point the solution at the previous step. The unilateral constraint is transformed in a barrier function.

The solution of the optimization routine is saved in a persistent memory, as a vector:

$$\mathbf{P} = [\mathbf{p}_{T,k} : k = 1..N]$$

Estimation

At this point, we could notice a lot of fluctuation in the solution, due to the noise in measurement, that is why we decided to treat the solution as a stochastic process. The solution are parsed in a *parzen window estimator*, a non-parametric estimator, that consider a kernel function $\gamma(\mathbf{p}, h)$ with volume $V(h)$:

- h identifies a kernel geometric characteristic
- the kernel is normal:

$$\int_{\mathbb{R}^n} \frac{\gamma(\mathbf{p}, h)}{V(h)} d\mathbf{p} = 1$$

- $\gamma(\cdot)$ has maximum in the origin
- $\gamma(\cdot)$ is continuous
- $\gamma(\mu \leftarrow \infty) \leftarrow 0$

the approximation of the distribution of the solution of the optimization step is in the form:

$$\hat{p}(\mathbf{p}) = \frac{1}{N} \sum_{k=1}^N \frac{\gamma(\mathbf{p} - \mathbf{p}_k, h)}{V(h)} \quad (3.46)$$

We have chosen as kernel a Gaussian function:

$$\int_{-\infty}^{\infty} \frac{1}{\sqrt{2\pi}h} e^{-\frac{z^2}{2h^2}} dz = 1$$

Such an estimator has the following drawbacks:

- with the exact knowledge of the distribution that we are trying to estimate, the expectation of the estimation shows us that such an estimation is a blurred version of the real one:

$$E\{\hat{p}(\mathbf{p})\} = p(\mathbf{p}) * \frac{1}{h} \gamma(\mathbf{p}, h)$$

- the estimation may suffer bias problem for samples $N < \infty$, that means

$$E\{\hat{p}(\mathbf{p})\} = E\{p(\mathbf{p})\} + \Delta$$

The final concept of the estimator is to identify the position inside a certain circle of confidence. When the drone is in such a confidence area, it release the dart to signal the position to the rescue.

4

Simulations

Contents

4.1	Implementations	69
4.1.1	Dynamic model	69
4.1.2	Receiver Model	70
4.1.3	Obstacle avoidance	71
4.1.4	Searching algorithm	71
4.2	Results	72

In this chapter we will see the implementation of part of the system using Matlab/Simulink platform. Some results are shown. Implementation takes into account the presence of noise in ARTVA receiver and consider a good estimation for the position and attitude of the system. To make simulation faster, we used C-compiled functions to perform heavier computational tasks.

4.1 Implementations

4.1.1 Dynamic model

The dynamic of the model is implemented with an S-Function, while the control is derived from the linearization of the model and thus inserted as gain in the model loop. The system has a free \hat{z} attitude, while position is controlled through the use of an integrated velocity vector.

The complete project is available online as a public Github repository. Please refer to the project for the actual source code of the single blocks.

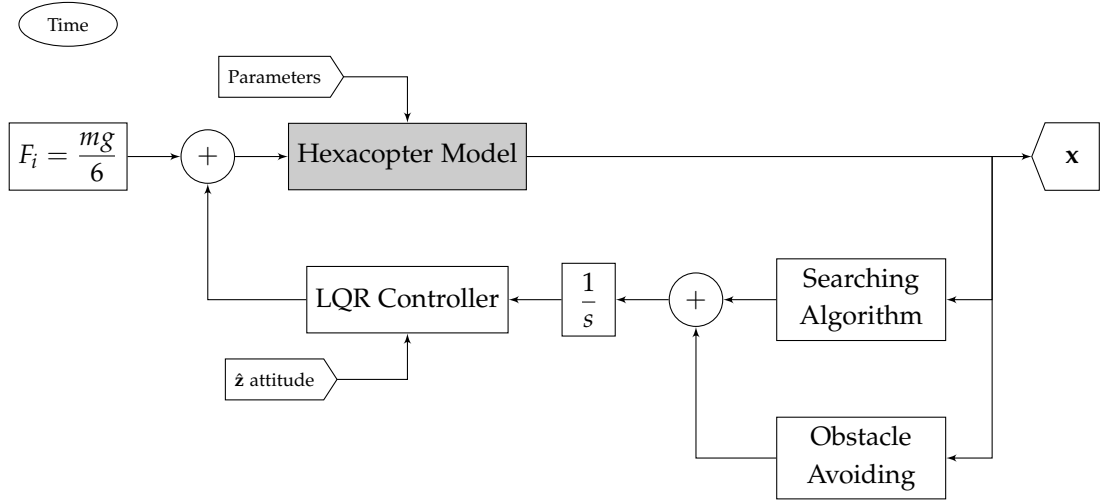


Figure 4.1: System complete model

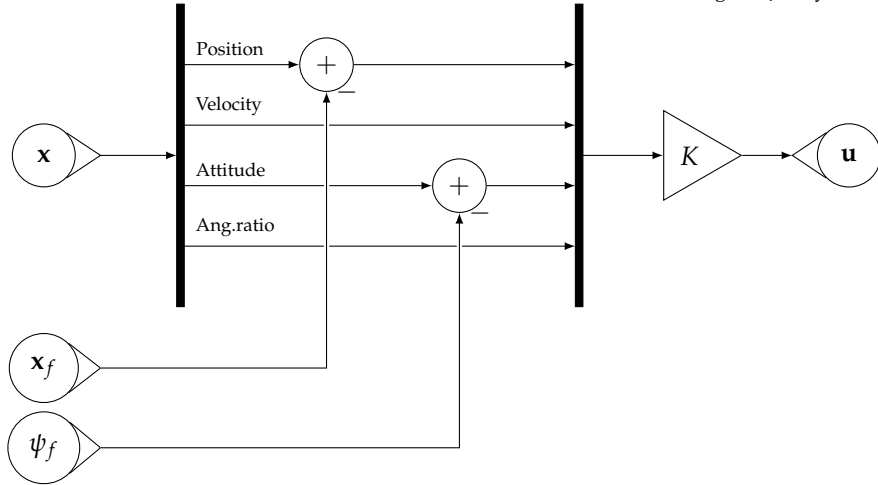


Figure 4.2: Tracking problem

4.1.2 Receiver Model

The receiver implements a mean sampler to reduce white Gaussian noise. The model of the receiver contains the equations of the H-field at which noise proportional to signal intensity on each antenna. The idea is to get 40dB of signal to noise ratio, that is quite optimistic, but it is also the value declared from some manufacturer. Also algorithm may work with lower receiver SNR.

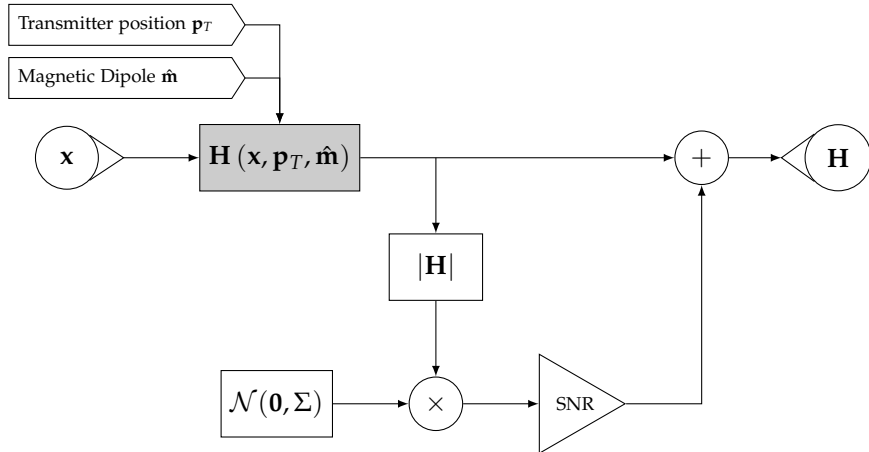


Figure 4.3: Receiver implementation

4.1.3 Obstacle avoidance

In the obstacle avoidance block we find a model of the receivers, written as a `mex`-function, and than the quite simple algorithm that allow us to avoid the obstacle generating a velocity vector orthogonal to the obstacle plane. This velocity vector is added to the searching input. This behavior is typical of the grounded paradigm.

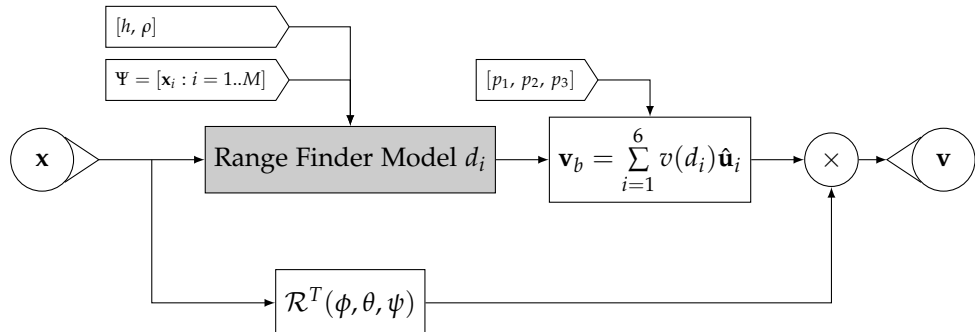


Figure 4.4: Obstacle avoidance sub-block

4.1.4 Searching algorithm

The receiver output feeds directly the two component of the source searching algorithm. The field information is transformed in an intensity and in a direction value to get an exploration direction. Measured field is used to perform the emulation, as an optimization problem. It was quite tricky to call the optimizer from Simulink, but possible using the `caller extrinsic` directive, alongside with an external evaluation from the Matlab engine, using `feval`. To speed up the process, residuals and barrier function results are evaluated using a `mex`-function. The parzen window estimation is performed offline, only as qualitative expression of the quality of the algorithm. The system shows some problem due to the symmetry of the transmitting field.

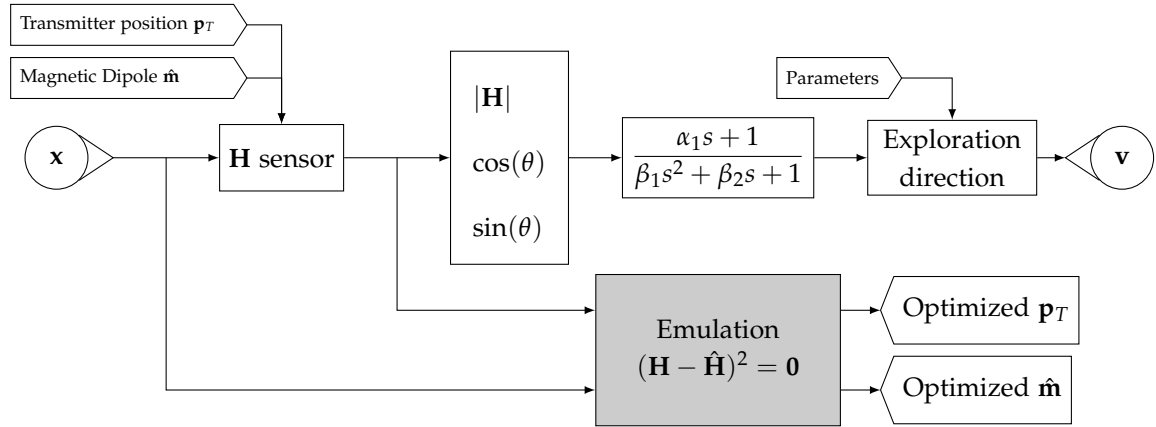


Figure 4.5: Searching algorithm sub-block

4.2 Results

In the next pages some results are reported, for a sample simulation.

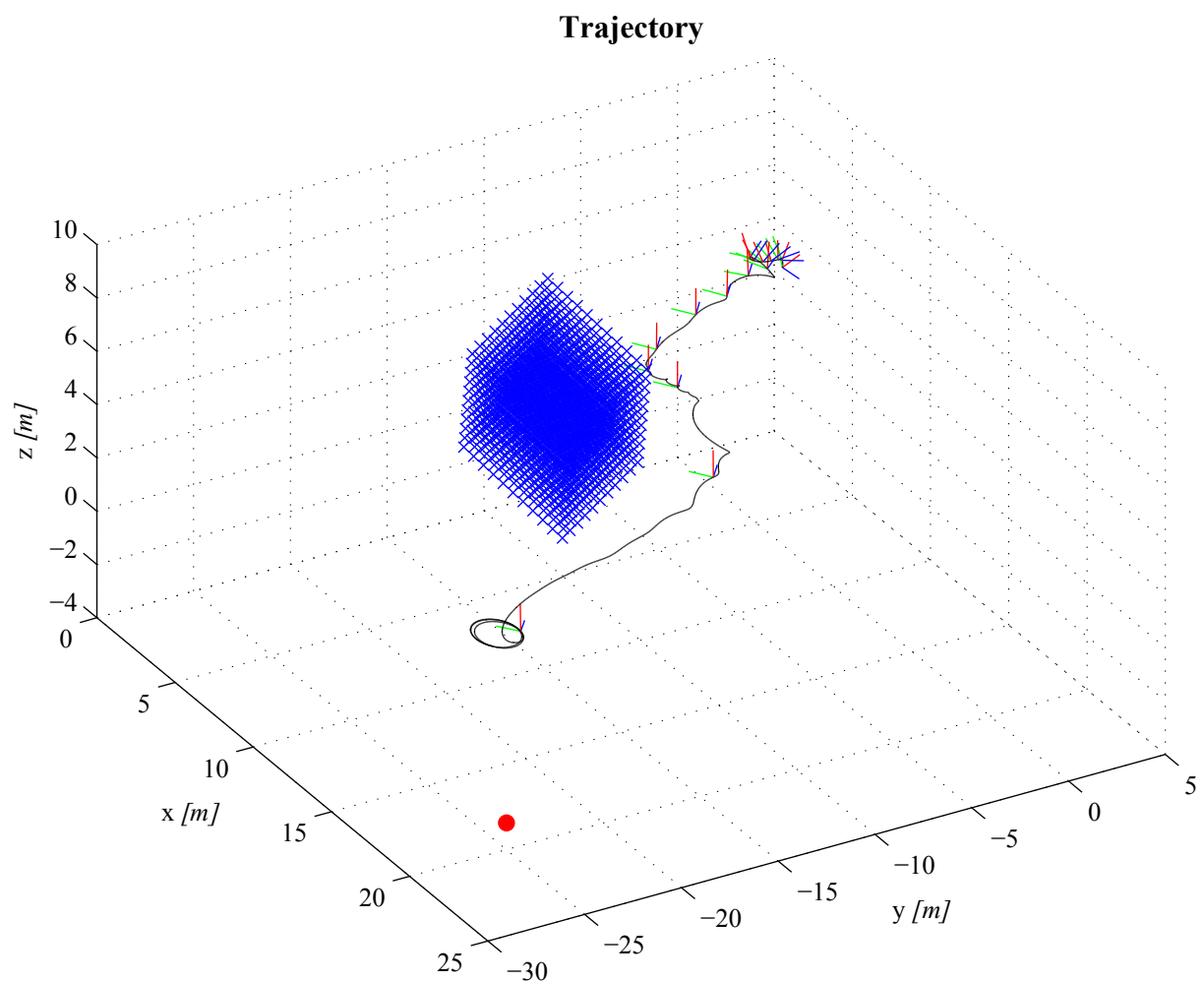


Figure 4.6: Graphical representation of a searching mission. The blue part is an obstacle, while the red dot is the position of the transmitter.

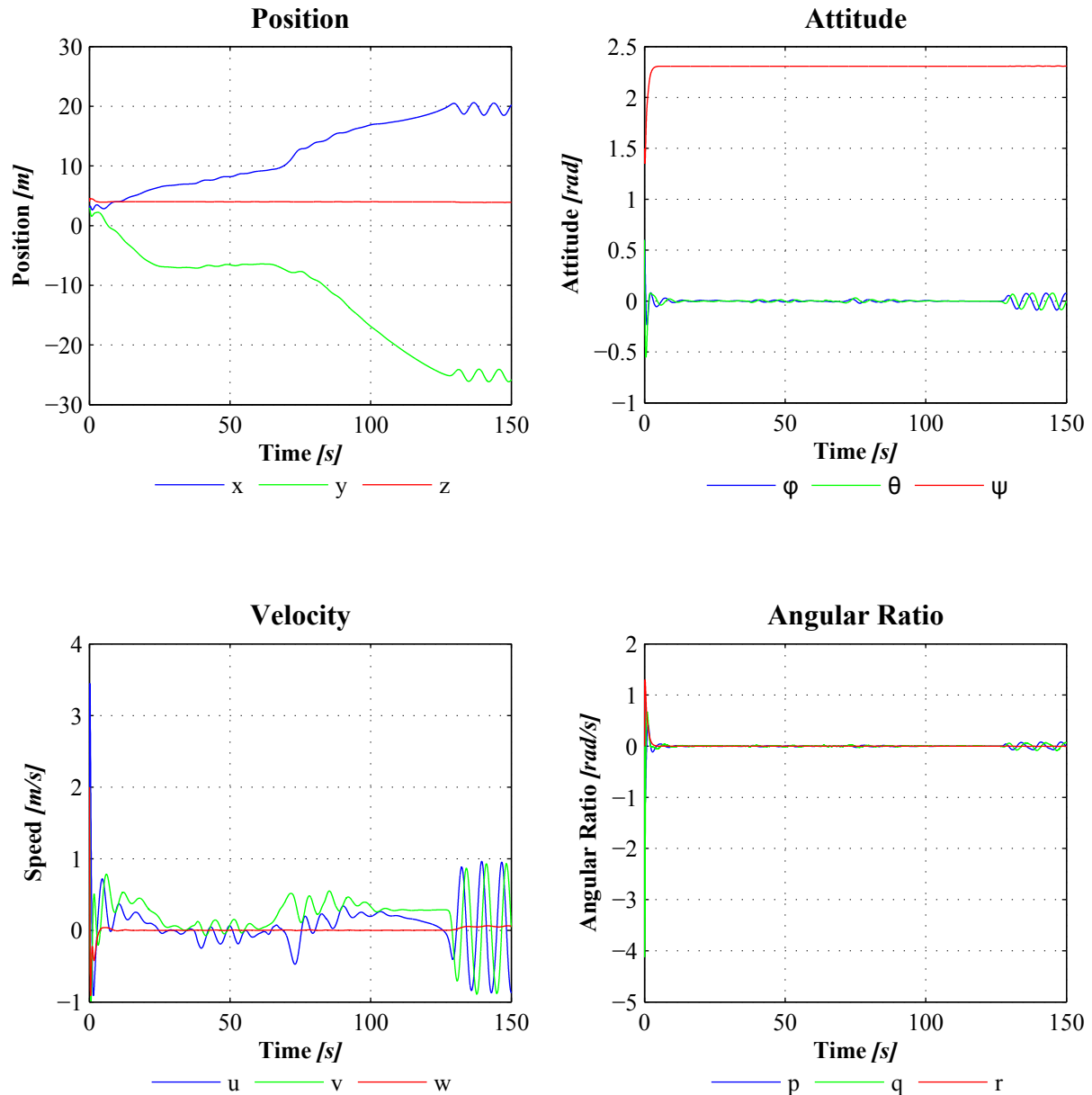


Figure 4.7: State of the drone during the entire searching routine. The earlier seconds are used to stabilize the drone, while for the rest of the time tries to reach the source.

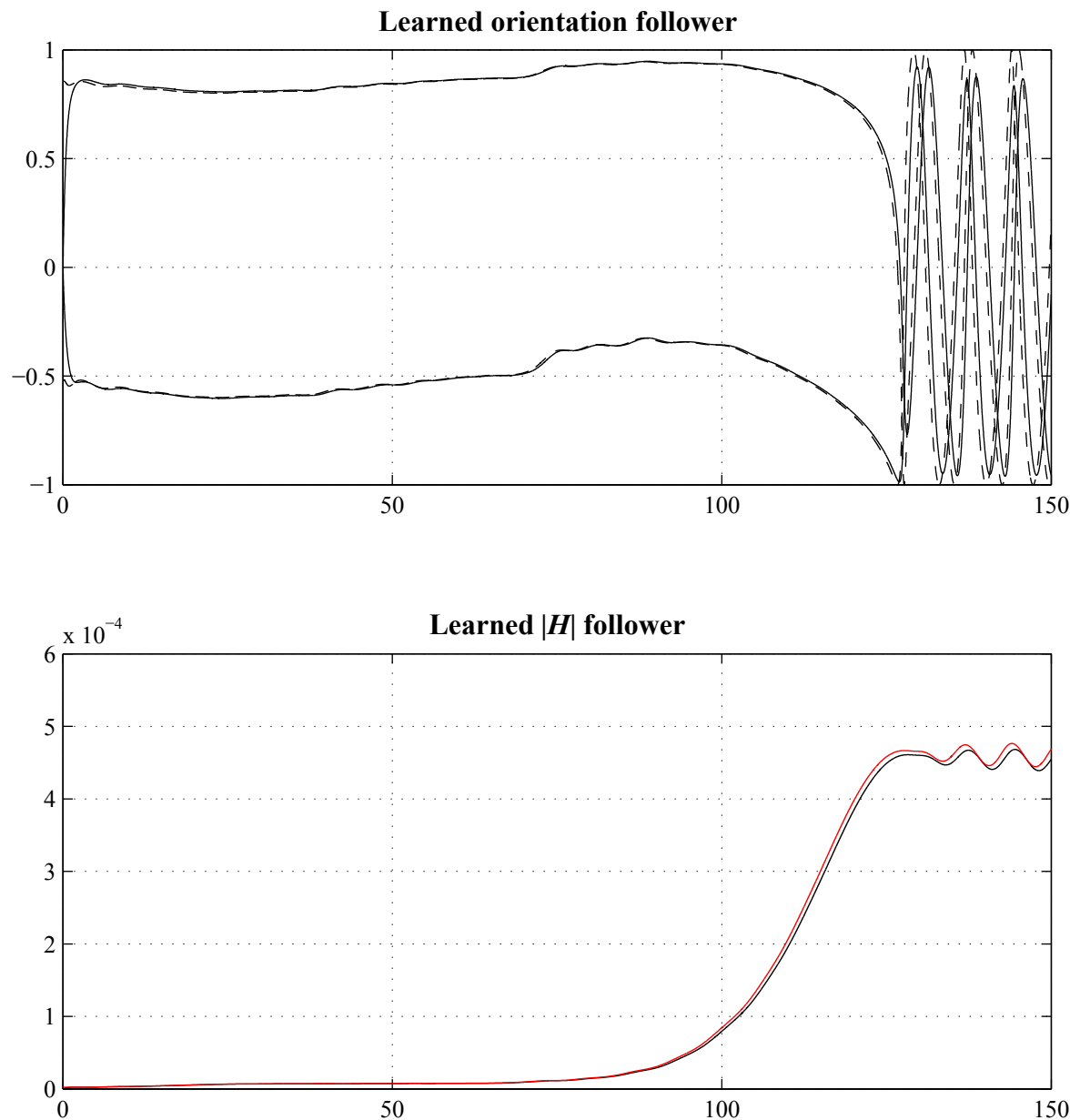


Figure 4.8: The searching routine perceived value. It is important to notice the monotonic behavior of the H -field strength. The algorithm succeeds in finding the direction in which the field increases.

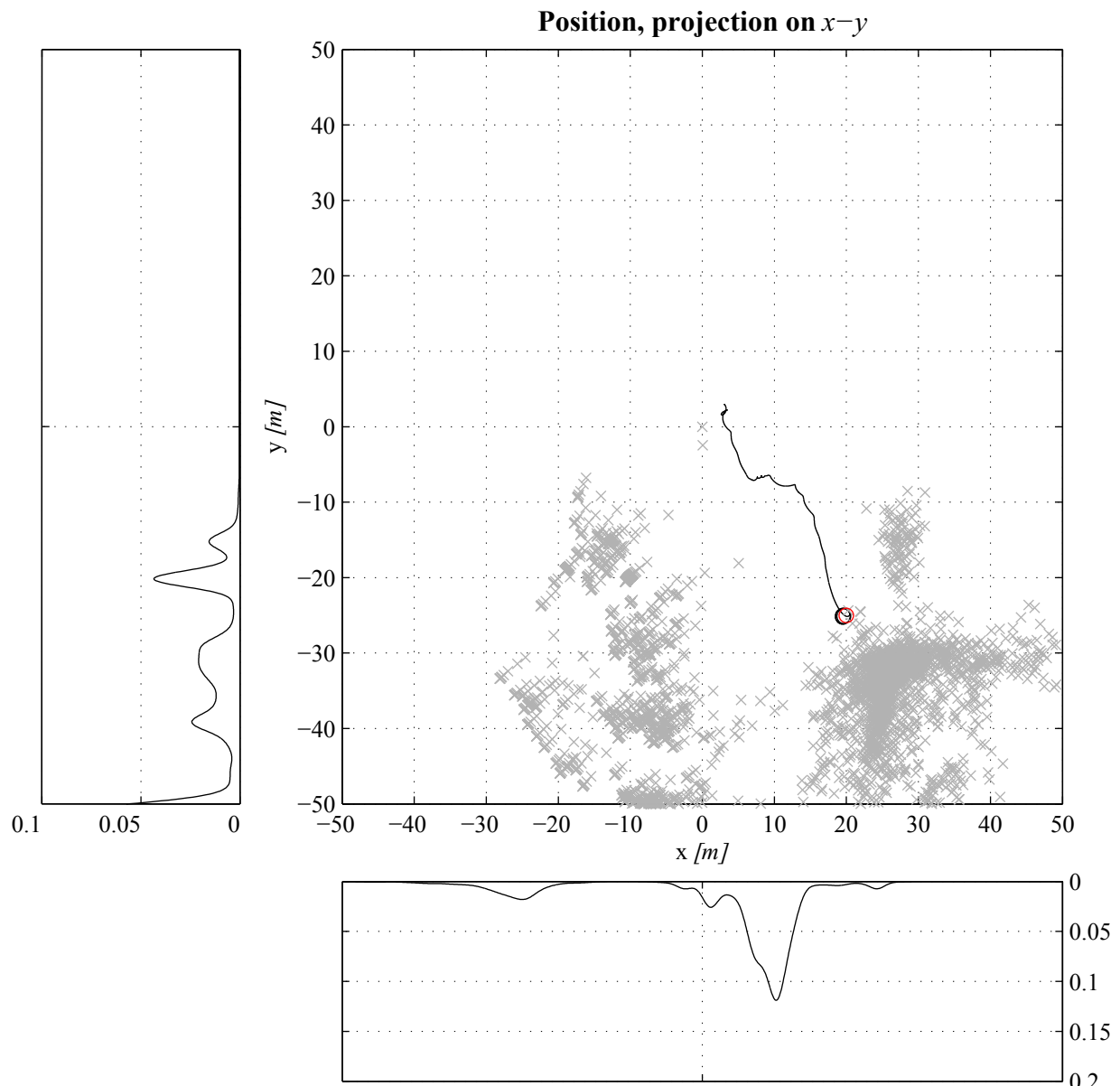


Figure 4.9: The results for the emulation routine. We can see that this algorithm does not produce great result at this time. We need to infer some more knowledge to the emulation equations. This problem could be related to the intrinsic symmetry of the field.

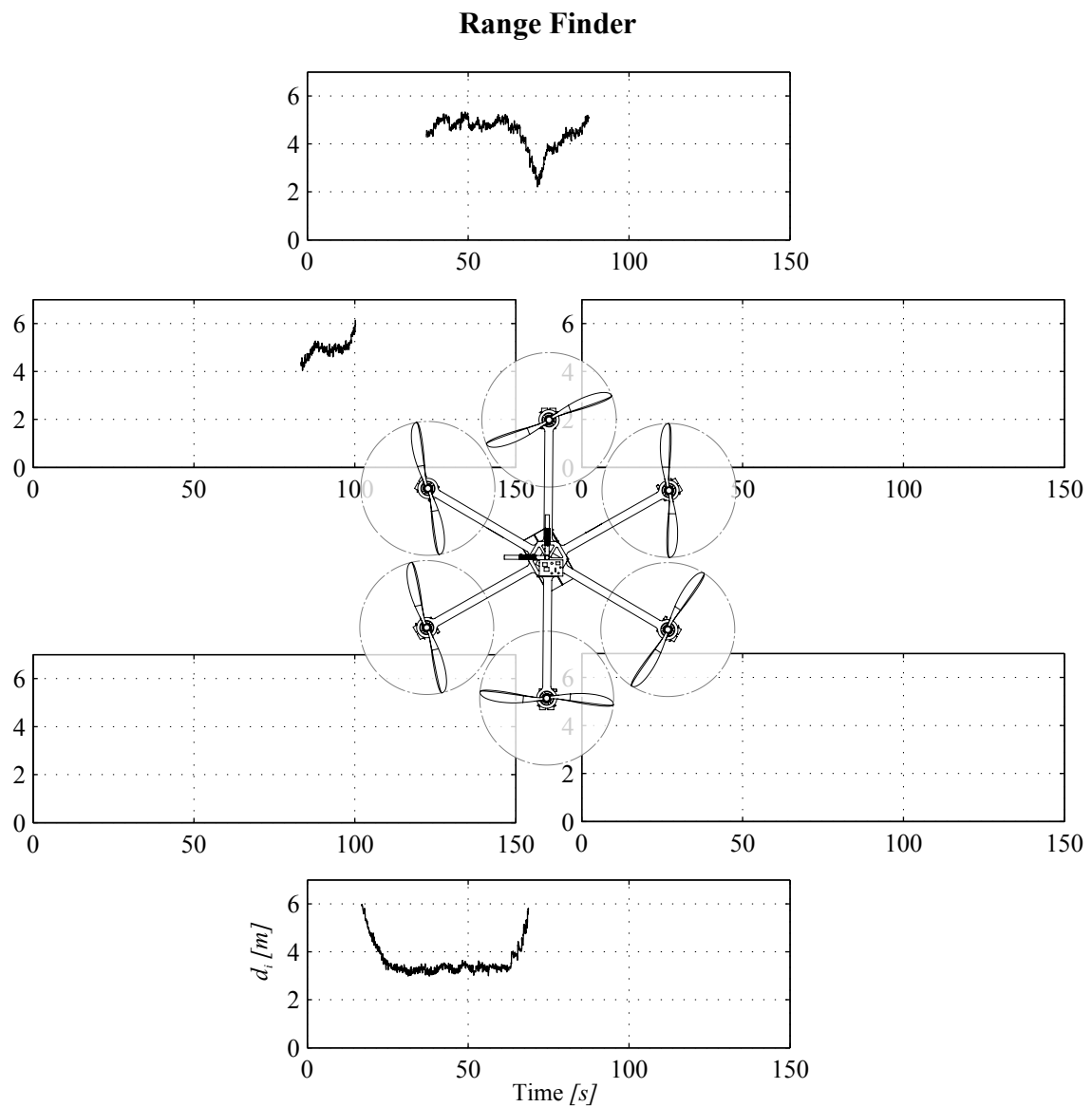


Figure 4.10: The range finder distance reading.

List of symbols

c	Speed of light
λ	Electromagnetic Wavelength
h_{eff}	Effective height of loop antenna
μ	Magnetic permeability
ϵ	Electric permittivity
\mathbf{r}	Radio distance vector
ρ	Charge density
\mathbf{J}	Current density
\mathbf{E}	Electric field
\mathbf{B}	Magnetic induction field
\mathbf{H}	Magnetic field
\mathbf{A}	Vector potential
ϕ	Scalar potential
ψ	Lorentz recalibration potential
ω_0	Transmitting angular frequency
ω_{int}	Transmitting intelligence angular frequency
\mathbf{m}	Magnetic dipole vector
κ	Wavenumber
\mathbf{p}_{tx}	Transmitter position
\mathbf{p}_{rx}	Receiver position
J_{int}	Intelligence signal current
J_{tx}	Transmitted signal current
Δ	Duty cycle
V_{ind}	Induced potential tension
N	Number of antenna coils
K	Boltzmann constant: $1.38 \times 10^{-23} \text{ J/K}$
$\mathcal{R}(\phi, \theta, \psi)$	Rotation matrix from body to ground
\mathbf{x}	Hexa-copter state vector
\mathbf{u}	Hexa-copter control vector
m	Mass of the drone
\mathbf{I}_b	Inertial matrix of the drone
\mathbf{F}	Total force on hexa-copter body
\mathbf{T}	Total torque on hexa-copter body

$\hat{\mu}$	State estimation in KF
\mathbf{z}	Measurement set in KF
$\bar{\mu}$	State prediction in KF
$\bar{\mathbf{z}}$	Measurement prediction in KF
Σ	State estimation covariance in KF
$\bar{\Sigma}$	State prediction covariance in KF
\mathbf{w}_t	State noise in KF
R_t	State noise covariance in KF
\mathbf{v}_t	Measurement noise in KF
Q_t	Measurement noise covariance in KF
K_t	Kalman Gain
\mathbf{s}	Radar detection signal
H_1	Signal present hypothesis
H_0	Signal absent hypothesis
$\Lambda(\mathbf{s})$	Signal decision likelihood ratio
η	Signal decision threshold
\mathbb{Z}	Decision space
\mathbb{Z}_1	Decision space signal present
\mathbb{Z}_0	Decision space signal absent
P_D	Probability of detection
P_M	Probability of missed alarm
P_C	Probability of correct rejection
P_F	Probability of false alarm
$\gamma(\mathbf{p}, h)$	Kernel function for parzen window estimator

Bibliography

- [1] ETSI EN 300 718-(1 2 3 4). E.r.m. avalanche beacons - transmitter-receiver systems. Technical report, ETSI, 2001.
- [2] Mizuno Shigeru Akao Yoji. *QFD: The customer-driven approach to quality planning and deployment*. Asian Productivity Organization, Tokio, J, 1994.
- [3] Constantine A Balanis. *Antenna theory: analysis and design*. John Wiley and Sons, 2012.
- [4] Randall D Beer. The dynamics of active categorical perception in an evolved model agent. *Adaptive Behavior*, 11(4):209–243, 2003.
- [5] Rodney A Brooks. A robust layered control system for a mobile robot. *IEEE Journal of Robotics and Automation*, 2(1):14–23, 1986.
- [6] Hermann Brugger, Hans Jürg Etter, Benjamin Zweifel, Peter Mair, Matthias Hohlrieder, John Ellerton, Fidel Elsensohn, Jeff Boyd, Günther Sumann, and Markus Falk. The impact of avalanche rescue devices on survival. *Resuscitation Journal*, 75(3):476–483, 2007.
- [7] Steve Christie. Having problems in multiple burial searches? signal overlap explained. *BackCountry Access*. From http://www.backcountryaccess.com/wp-content/uploads/2014/02/Signal_Overlap.pdf.
- [8] Mauro Da Lio, Francesco Biral, Enrico Bertolazzi, Marco Galvani, Paolo Bosetti, David Windridge, Andrea Saroldi, and Fabio Tango. Artificial co-driver as a universal enabling technology for future intelligent vehicles and transportation systems. *Transaction on Intelligent Transportation Systems*, To Be Published.
- [9] Stevan Harnad. The symbol grounding problem. *Physica D: Nonlinear Phenomena*, 42(1):335–346, 1990.
- [10] John Hereford and Bruce Edgerly. 457 khz electromagnetism and the future of the avalanche transceiver. *BackCountry Access*. From https://s3.amazonaws.com/BackcountryAccess/content/papers/457andFuture_000.pdf.

- [11] John Hereford and Bruce Edgerly. Digital transceiving systems: the new generation of avalanche beacons. *BackCountry Access*. From https://s3.amazonaws.com/BackcountryAccess/content/papers/DigitalSys_NextGeneration.pdf.
- [12] Chuck Hutchinson et al. *The ARRL handbook for radio amateurs*. American Radio Relay League, 2000.
- [13] Repubblica Italiana. Legge 24/12/2003 n. 363. *Gazzetta Ufficiale*, 2003.
- [14] Thomas Lund. Signal strength versus signal timing: Achieving reliability in multiple burial searches. *BackCountry Access*. From https://s3.amazonaws.com/BackcountryAccess/content/papers/SignalOverlapPaper_001.pdf.
- [15] Luc Oth Manuel Grauwiler. Fully autonomous search for avalanche victims using an mav, 2010.
- [16] Pedro Piniés and Juan D Tardós. Fast localization of avalanche victims using sum of gaussians. In *Proceedings of IEEE International Conference on Robotics and Automation*, pages 3989–3994. IEEE, 2006.
- [17] Pedro Piniés, Juan D Tardós, and José Neira. Localization of avalanche victims using robocentric slam. In *IEEE/RSJ International Conference on Intelligent Robots and Systems*, pages 3074–3079. IEEE, 2006.
- [18] CD Salös, FM Lera, and JL Villarroel. Digital signal processing in triple antenna arvas. In *IEEE International Conference on Signal Processing and Communications*, pages 484–487. IEEE, 2007.
- [19] Mikhail Shevchenko, David Windridge, and Joseph Kittler. A linear-complexity reparameterisation strategy for the hierarchical bootstrapping of capabilities within perception-action architectures. *Image and Vision Computing*, 27(11):1702–1714, 2009.
- [20] Ron Sun, Edward Merrill, and Todd Peterson. From implicit skills to explicit knowledge: A bottom-up model of skill learning. *Cognitive Science*, 25(2):203–244, 2001.
- [21] Aa. Vv. *Club Alpino Italiano - Manuale Sci Alpinismo*. Commissione Pubblicazioni CAI, 2004.
- [22] David Windridge, Michael Felsberg, and Affan Shaukat. A framework for hierarchical perception-action learning utilizing fuzzy reasoning. *IEEE Transactions on Cybernetics*, 43(1):155–169, 2013.